Petrological and noble gas features of Lascar and Lastarria volcanoes (Chile): Inferences on plumbing systems and mantle characteristics

Article *in* Lithos · June 2020

DOI: 10.1016/j.lithos.2020.105615

8 authors, including:

Philippe Robidoux
University of Chile
21 PUBLICATIONS **120** CITATIONS
SEE PROFILE

Andrea Luca Rizzo
National Institute of Geophysics and Volcanology
160 PUBLICATIONS **1,519** CITATIONS
SEE PROFILE

Felipe Aguilera
Universidad Católica del Norte (Chile)
142 PUBLICATIONS **551** CITATIONS
SEE PROFILE

Mariano Artale
Università degli Studi di Palermo
3 PUBLICATIONS **0** CITATIONS
SEE PROFILE

Lithos 370–371 (2020) 105615

Contents lists available at ScienceDirect

Lithos

journal homepage: www.elsevier.com/locate/lithos

Research Article

Petrological and noble gas features of Lascar and Lastarria volcanoes (Chile): Inferences on plumbing systems and mantle characteristics

P. Robidoux [a,*], A.L. Rizzo [b], F. Aguilera [c,d,e], A. Aiuppa [f], M. Artale [f], M. Liuzzo [b], M. Nazzari [g], F. Zummo [f]

[a] Centro de Excelencia en Geotermia de los Andes (CEGA) y Departamento de Geología, Facultad de Ciencias Físicas y Matemáticas, Universidad de Chile, Plaza Ercilla 803, Santiago, Chile
[b] Istituto Nazionale di Geofisica e Vulcanologia, Sezione di Palermo, Via Ugo La Malfa, 153, Palermo, Italy
[c] Departamento de Ciencias Geológicas, Universidad Católica del Norte, Avenida Angamos 0610, Antofagasta, Chile
[d] Núcleo de Investigación en Riesgo Volcanico - Ckelar Volcanes, Universidad Católica del Norte, Avenida Angamos 0610, Antofagasta, Chile
[e] Centro de Investigación para la Gestión Integrada del Riesgo de Desastres (CIGIDEN), Vicuña Mackenna 4860, Santiago, Chile
[f] Dipartimento DiSTeM, Università di Palermo, Via Archirafi 36, Palermo, Italy
[g] Istituto Nazionale di Geofisica e Vulcanologia, Sezione Roma, Via di Vigna Murata, 605, Rome, Italy

ARTICLE INFO

Article history:
Received 11 January 2020
Received in revised form 29 May 2020
Accepted 30 May 2020
Available online 08 June 2020

Keywords:
Lascar
Lastarria
Noble gases
Fluid inclusions
Crustal contamination
Mantle wedge

ABSTRACT

Lascar (5592 m a.s.l.) and Lastarria (5697 m a.s.l.) are Chilean active stratovolcanoes located in the Central Volcanic Zone (CVZ; 16°S to 28°S) that have developed on top of a 71 km thick continental crust. Independently of the similarities in their Plinian/Vulcanian eruptive styles, their complex magmatic feeding structures and the origins of their magmatic fluids still necessitate constraints in order to improve the reliability of geochemical monitoring. Here we investigate the petrography, bulk-rock chemistry, and mineral chemistry in products from the 1986–1993 explosive eruptive cycle at Lascar and from several Holocene eruptive sequences at Lastarria. These data are integrated with measurements of the noble gas isotopes in fluid inclusions (FIs) of minerals from the same products as well as in fumarole gases. The geochemistry of minerals and rocks shows that the studied products belong to high-K–calc-alkaline series typical of subduction-related settings, and provide evidence of differentiation, mixing, and crustal assimilation that are higher at Lastarria. The contribution of slab sediments and fluids to magma genesis in the wedge is limited, suggesting a homogeneous mantle beneath CVZ. The deepest crystallization processes occurred at variable levels of the plumbing systems according to the lithostatic equivalent depths estimated with mineral equilibrium geobarometers at Lascar (15–29 km) and Lastarria (~20–40 km). The $^{40}Ar/^{36}Ar$ and $^{4}He/^{20}Ne$ ratios in FIs and fumarole gases indicate the presence of some degree of air contamination in the fluids from both volcanoes. The $^{3}He/^{4}He$ values at Lascar (6.9–7.3 Ra) are relatively homogeneous and comparable to those of fumaroles, suggesting a main zone of magma crystallization and degassing. In contrast, the $^{3}He/^{4}He$ values at Lastarria (5.31–8.01 Ra) vary over a wide range, suggesting various magma storage levels and providing evidence of crustal contamination, as indicated by the rock chemistry. We argue that mantle beneath the two volcanoes has a MORB-like signature of $^{3}He/^{4}He$, while local crustal contamination explains the lower ratios measured at Lascar.

1. Introduction

Lascar and Lastarria (Chile) are two of the most actively degassing stratovolcanoes in the Central Volcanic Zone of the Andes (CVZ) (Tamburello et al., 2014), and they have a long record of volcanic eruptions with magnitudes up to Plinian/Vulcanian. Lascar erupted frequently during historic time (González-Ferrán, 1995) and continued to present time as testified by recent signs of activity with the occurrence of phreatic explosions from October 2015 (Gaete et al., 2019; Gaete Rojas et al., 2020; Global Volcanism Program, 1996). A short-lived magmatic intrusive event was responsible for major explosive eruptions in 1993 (Calder et al., 2000; Gardeweg et al., 1998, 2011; Matthews et al., 1994). Lastarria does not have a historical record of eruptive activity but has exhibited major explosive eruptions during the Holocene (Naranjo, 1992). The time intervals separating the major explosive events could have lasted between 1660 and 2390 ± 40 yr according to uncalibrated accelerator mass spectrometry (AMS) measurements on ^{14}C radiocarbon dating of organic sediments found along deposits of avalanche and ignimbrites (Naranjo, 2010).

The available petrological and geophysical information indicates that the two volcanoes have complex plumbing systems and different magma residence times in crustal reservoirs (Aguilera et al., 2012; Naranjo, 2010). At Lascar, for example, the 1993 eruptive products are

* Corresponding author at: Centro de Excelencia en Geotermia de Los Andes CEGA, Departamento de Geología, Facultad de Ciencias Físicas y Matemáticas, Universidad de Chile, Santiago, Chile.
E-mail address: robidouxphilippe@gmail.com (P. Robidoux).

https://doi.org/10.1016/j.lithos.2020.105615
0024-4937/

thought to have erupted from the superficial (~2 km deep) magma ponding zone, while increasing works on seismic monitoring extend the presence of the actual conduit down to a depth of ~5 km (Gaete et al., 2019; Gaete Rojas et al., 2020). Mineral–melt equilibria imply a vertically elongated plumbing system extending as deep as 11.5 km (up to ~500 MPa; Stechern et al., 2017). At Lastarria, seismic tomography has indicated that magma could actually be stored from as shallow as ~1 km to as deep as 5–6 km (Spica et al., 2015).

Although considering numerous studies, the complex magmatic feeding systems and the origin of magmatic volatiles remain only partially understood at both volcanoes. In addition, despite the volcanoes being located at the edge of the Andean subduction zone above ~71 km thickness of rigid continental crust (Thorpe, 1982), the impact of crustal assimilation on the composition of intruding magma is poorly understood. It remains unclear whether the magmatic fluids that today feed fumarole emissions originate from fresh and undegassed newly ascending magma or from more-aged and cooling stored melts.

In this work, we combine petrological data with noble-gas analyses of fluid inclusions (FIs) in olivines and clinopyroxenes (Cpx) of rocks erupted from Lascar and Lastarria volcanoes. The chemistry of the mineral assemblage is integrated with analyses of bulk-rock major and trace elements to address some of the above open questions on the levels of magma storage below the volcanoes. We also attempt to identify possible differences between the two plumbing systems, and the role of continental crust thickness in contaminating magma compositions. The novel data of He-Ne-Ar elemental concentration and isotopic ratios in FIs of rocks from Lascar and Lastarria, integrated by the same measurements in fumarole gases from Lastarria, are compared to the existent data of fumarole gases from the two volcanoes to constrain the $^{3}He/^{4}He$ signatures of the local magmatic sources. These signatures are finally compared to similar measurements carried out in other Central and South American volcanoes to assess whether any $^{3}He/^{4}He$ values difference between Lascar and Lastarria can be imputable to crustal contamination or mantle heterogeneities.

2. Geological and geodynamic setting

Orogenic andesitic stratovolcanoes from the Neogene to the present day along the South American Volcanic Arc are structurally and compositionally grouped in three main zones from north to south: (1) Northern Volcanic Zone (5°N to 2°S), (2) CVZ (16°S to 28°S), and (3) Southern Volcanic Zone (33°S to 52°S) (Harmon et al., 1984; Thorpe, 1982; Thorpe and Francis, 1979). From north to south, the crust thickness varies between 71 and 30 km. The variable depth of the Benioff plan (80–120 km) plays a major role in delivering slab fluid and the partial melting of the mantle wedge, while crustal assimilation impacts the K content of the magma (Stern, 2004), contributing to defining calc-alkaline (CA) versus shoshonitic volcanic rock series (Stern, 2004). The convergence rate averages 7 cm/year (DeMets et al., 2010) and trench structures vary from deep, dry, and sediment-poor in the north, to shallow and sediment-rich in the south (Völker et al., 2013).

2.1. Chemistry of CVZ magmas

Magmas in the Andean CVZ are mainly andesites to dacites, but some mafic (i.e. Godoy et al., 2019) and felsic endmember magmas have also been found (Wörner et al., 2018 and references therein). The continental crust contamination is significant in CVZ magmas as testified by their higher $^{87}Sr/^{86}Sr$, $^{207}Pb/^{204}Pb$, and $^{208}Pb/^{204}Pb$ ratios, and lower $^{143}Nd/^{144}Nd$ ratios than in the rest of the South American Volcanic Arc (e.g., Davidson and de Silva, 1992; De Silva and Francis, 1991; Harmon et al., 1984; Haschke et al., 2006; Hickey et al., 1986; Hildreth and Moorbath, 1988; Jacques et al., 2014; Kay et al., 2014; Mamani et al., 2008, 2010; Scott et al., 2018; Thorpe, 1984; Wörner et al., 1994; Wörner et al., 2018). Overall, the Sr and Pb isotope concentrations decrease (and the Nd concentrations increase) with the age of the CVZ rocks, except for the majority of the Mesozoic volcanic fields and ignimbrites that include evolved endmembers (De Silva et al., 2006).

The patterns of rare earth elements (REE) are typical of volcanic arc settings, but indicate frequent heterogeneities with N-MORB, *E*-MORB, and OIB signatures due to large variations in different accreted terrains (Mamani et al., 2008, 2010 and references therein). Specific trace element ratios mark an important crustal contribution to magmatism in volcanic rocks from CVZ (high Sr/Y, La/Yb, etc.; Mamani et al., 2008; Chiaradia, 2015) and underline small slab fluid and sediment inputs to magma genesis (low Ba/La, Sr/Nd, Th/La, U/Th; Workman and Hart, 2005; Plank and Langmuir, 1998; Plank, 2014).

2.1.1. Lascar volcano

Lascar volcano (23.37°S and 67.73°W, 5592 m a.s.l.) is a stratovolcano located in the central part of the CVZ (Fig. 1). This volcano comprises two cones hosting five nested craters trending along an ENE–WSW direction. The central crater is the currently active vent and is characterized by intense fumarole activity. Records of eruptive activity date back to the 19th century and cover more than 40 eruptions (e.g., Aguilera et al., 2006 and references therein). The activity was most intense between 1984 and 1994, when three main dome growth-and-collapse cycles generated lava domes that were successively destroyed by moderate Vulcanian eruptions (Matthews et al., 1997).

The most-prominent event recorded in historical time was the 1993 sub-Plinian eruptive phase. The eruption emitted 0.1 km^3 of rocks, generating eruptive columns that reached up to 25 km, pyroclastic flows going down the NW and SE flanks extending as far as 8 km from the active crater (Gardeweg and Medina, 1994), and falls of tephra that were detected in Argentina, Paraguay, Brazil, and Uruguay (Global Volcanism Program, 1993, 1994). The last explosion was recorded on October 30th 2015, whose eruptive column reached 2.5 km above the active crater (Global Volcanism Program, 2015). A permanent gas plume is still emitted from the active crater (Global Volcanism Program, 2017, 2018), where highly variable SO_2 fluxes have been recorded during 1989–2013, ranging between 150 and 2300 tons/day (e.g., Andres and Kasgnoc, 1998; Bredemeyer et al., 2018; Layana et al., 2020; Menard et al., 2014; Tamburello et al., 2014).

According to Gardeweg et al. (1998, 2011), Lascar volcano is built over a basement constituted by a series of volcanic/volcaniclastic/sedimentary sequences intruded by granitoids rocks from Permian to Miocene. Upper Miocene to Pleistocene strata of ignimbrites with

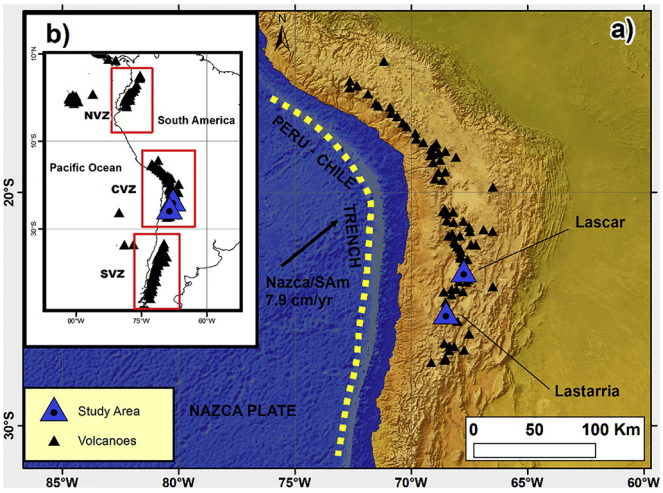

Fig. 1. Locations. Topographic map and locations of the analyzed volcanoes. (a) Converging Nazca and South America plates (Nazca/SAm) with its subduction vector illustrated using a black arrow representing the NUVEL 1-A model from DeMets et al. (1994). (b) Continental-scale map showing the North Volcanic Zone (NVZ), CVZ, and South Volcanic Zone (SVZ).

important thickness, domes, and volcanic rocks follow the sequence (Gardeweg et al., 1998). Gardeweg et al. (2011) divided the evolution of Lascar volcano over the basement into four stages ranging from ca. 240 ky up to the present day (Calder et al., 2000; Gardeweg et al., 1998).

The eruptive products emitted from Lascar volcano belong to moderate-to-high K-CA series. Their $^{87}Sr/^{86}Sr$ (0.7057–0.7071), $^{143}Nd/^{144}Nd$ (0.51240–0.51244) isotopic ratios, all measured in andesitic lavas and strictly emitted from Lastarria crater all suggest a moderate crustal contamination (Mamani et al., 2008, 2010; Trumbull et al., 1999). We do not report data on Negria lava field, whose center of emission is different (Rosner et al., 2003 and Wittenbrink, 1997 cited in Rosner et al., 2003). The isotopic ratios of $^{207}Pb/^{204}Pb$ (15.62–15.64), $^{206}Pb/^{204}Pb$ (18.74–18.84), and $^{208}Pb/^{204}Pb$ (38.66–38.84) fall within most of CVZ datasets (Harmon et al., 1984; Hilton et al., 1993; Mamani et al., 2010; Rosner et al., 2003). Although the lead isotopes are representative of relatively radiogenic mantle values (Rosner et al., 2003), they also highlight evidence of crustal contamination similar to most volcanic centers grouped in the Antofalla domain, as defined on the basis of the isotopic composition of basement rocks and contaminated arc magmas from the Andean crust by Mamani et al. (2008, 2010).

2.1.2. Lastarria volcano

Lastarria volcano (25.16°S and 68.50°W, 5697 m a.s.l.) is a composite stratovolcano located in the southern part of the CVZ (Fig. 1). It forms part of a major volcanic structure called the Lastarria Volcanic Complex (LVC), which also includes the Southern Spur volcano and the Negriales lava field (Naranjo, 2010). Lastarria is a single edifice (~10 km^3) constituted by five nested craters that are aligned along a north–south direction. Four permanent fumarole fields are currently located along the rim of crater 4, inside crater 5, and on its northwestern flank, each covering 0.001–0.04 km^2 and characterized by intense fumarole activity (Fig. 1b; Aguilera, 2008).

Lastarria volcano has undergone ground deformation and been characterized by a long period of earthquakes since at least 1997 (Froger et al., 2007; Pritchard and Simons, 2004). A major deformation is centered on the so-called Lazufre area (constituting the LVC, Cordón del Azufre, and Bayo volcanoes), with a depth of 7–15 km and a deformation rate of 2–3 cm/year, with some areas related to an overpressure source (e.g., boiling aquifer) lying 1000 m below the crater area (Budach et al., 2013; Díaz et al., 2015; Froger et al., 2007; Pritchard and Simons, 2002; Ruch et al., 2009; Spica et al., 2015).

The LVC has produced Upper Miocene/Upper Pleistocene andesitic-to-dacitic lava flows and domes, with subordinate basaltic andesite lava flows (Naranjo, 1992, 2010). Pyroclastic rocks corresponding to Lower Pleistocene dacitic ignimbrites are also present.

Naranjo (2010) summarized the geological evolution of the LVC into three major volcanic structures: (1) Negriales lava field (400 ± 60–116 ± 26 ky [mean ± SD]; Middle to Upper Pleistocene), (2) Espolón Sur (Southern Spur) (150 ± 50 ky; Middle Pleistocene), and (3) Lastarria sensu stricto. Naranjo divided the evolution of the LVC into 10 stages ranging from 330 ± 100 to 249 ± 36 ky (Middle Pleistocene) up to the Holocene and present day.

The eruptive products from Lastarria volcano belong to high-K calc-alkaline (HK-CA) series (Mamani et al., 2008, 2010; Naranjo, 2010). In andesitic lavas, Trumbull et al. (1999) and Mamani et al. (2008) reported the isotopic ratios of $^{87}Sr/^{86}Sr$ (0.7069–0.7072) and $^{143}Nd/^{144}Nd$ (0.512442–0.512446), suggesting different extents of crustal contamination (Mamani et al., 2008, 2010). The isotopic ratios of $^{207}Pb/^{204}Pb$ (15.59–15.70), $^{206}Pb/^{204}Pb$ (18.81–18.92) and $^{208}Pb/^{204}Pb$ (38.63–39.07)(Mamani et al., 2010; Rosner et al., 2003), being among the highest isotopic ratios among the crustal domains defined by Mamani et al. (2008, 2010), all support that Lastarria rocks represent a mantle signature strongly contaminated by intracrustal assimilation.

3. Sampling and methods

3.1. Sampling locations

The scientific approach used in this work implied two main conditions in the selection of the suite of samples: 1) the necessity of sampling rocks as much mafic as possible in order to separate olivine and clinopyroxene for noble gas measurements in fluid inclusions as well as for reasonable petrological reconstruction of the pristine magmatic composition and plumbing system structure. This is never easy in arc volcanoes developed on thick continental crust, as for Lascar and Lastarria. 2) The attempt to extend back in time as much as possible the age of the erupted rocks for evaluating any temporal modification of the magmatic composition and plumbing system, without losing the opportunity of comparing it with present day activity and degassing. These conditions dramatically reduced the number of suitable samples.

3.1.1. Rocks

The Lascar rock samples LAS1, LAS2, and LAS3 are crystal-rich scoriae from pyroclastic-flow deposits emitted from the central crater (Table 1). The youngest material collected was emitted during the sub-Plinian eruption in April 18–21, 1993 (Matthews et al., 1994; Sparks et al., 1997; Calder et al., 2000). Distant pyroclastic deposits located on the northwestern flank were found to be abundant in white pumices (Matthews et al., 1994) and dark-colour clasts of large scoriae bombs and crystalline blocks (up to 1 m). The white and vesicular pumices (described and studied by Matthews et al., 1994; Sparks et al., 1997; Calder et al., 2000) were not collected because they are not associated with the mafic juvenile source and do not contain large quantities of visible olivines and pyroxenes. Our sampling thus preferentially targeted the dark scoriae with sizes ranging from lapilli to bombs and grey block fragments of the pyroclastic-flow deposits. More specifically, we present data for the crystalline porphyric dome fragments emitted during 1986–1993 (LAS1) and juvenile scoriae (LAS2) (Matthews et al., 1994).

We also studied the Tumbres scoria flow deposit (pyroclastic flow in Gardeweg et al. (1998) (ca. 9.2 ky; Gardeweg et al., 2011) sampled in outcrops in the southern Tumbres area and in the Talabre Viejo canyon. This sampling site corresponds to the northeastern border of the flow, and several fragments weighing >3 kg were taken from large scoriae bombs (LAS3). Textures were similar to LAS2 scoriae, but the LAS3 scoriae presented alternating grey and beige surfaces. Full details on the locations of the deposits are presented in Table 1.

Sampling at Lastarria was performed on the northwestern flank and concentrated on Holocene pyroclastic-flow deposits containing scoriaceous lapilli and bombs, banded black and beige pumices, and lithic block components (Table 1; Naranjo, 2010). LRA1 and LRA2 are scoriae fragments with sizes ranging from lapilli to bombs that fall under the "grey IV pyroclastic flow deposit" definition reported by Naranjo (1992), grouped here as "Ignimbrite 3" (Naranjo, 2010) (Table 1 provides a list of equivalent names). This flow was emitted by crater 4, where most of the actual summit fumaroles are located (Aguilera, 2008). The pyroclastic deposit is dated 2.46 ± 0.04 ky A.P. (Naranjo, 2010). The LRA3 sample consists of dark crystalline pumice fragments found between the contact of Ignimbrite 1 and 3 (Naranjo, 2010), corresponding petrographically and geographically to the "grey I pyroclastic flow deposit" defined by Naranjo (1992). This association chronologically relate the deposit to late Holocene (~2.5–4.8 ky) (Naranjo, 2010). The LRA4 rock samples are pale crystalline pumice fragments emitted by crater 3, which is older. From the position of the sampling site, petrographic features, and stratigraphic position (the fragments are white pumices covering the superior layer of the flow margin), we infer that LRA4 is associated with the 4.85 ± 0.04 ky A.P. Ignimbrite 1 described in Naranjo (2010), and more specifically with the "pink pyroclastic flow deposit" defined by Naranjo (1992).

Table 1
Sample location and coordinates along with field and sample petrographic descriptions.

Sample ID	Volcano	Long (deg.)	Lat (deg.)	Alt. (m)	Material	Name - (Naranjo, 1992)	Name - Naranjo (2010)	Chronology
LRA1	Lastarria	25° 9′17.11"S	68°31′32.36"O	4992	Scoriae	Grey IV pyroclastic flow deposit	Ignimbrite 3	>Holocene
LRA2	Lastarria	25° 9′17.11"S	68°31′32.59"O	4992	Scoriae	Grey IV pyroclastic flow deposit	Ignimbrite 3	>Holocene
LRA3	Lastarria	25° 9′7.65"S	68° 31′47.44"O	4697	Pumice fragments	Grey I pyroclastic flow deposits (?)	Contact Ignimbrite 1–3	>Holocene
LRA4	Lastarria	25° 9′7.67"S	68° 32′7.59"O	4558	Pumice fragments	Pink pyroclastic flow deposit	Ignimbrite 1	>Holocene
LAS1	Lascar	23° 18′46.61"S	67° 47′0.67"O	3919	Dome fragment	Pyroclastic flow deposit, 1993	–	1986–1993, (emitted, 1993)[b]
LAS2	Lascar	23° 18′45.09"S	67° 47′2.20"O	3925	Scoriae	Pyroclastic flow deposit, 1993	–	1993, April 19–21
LAS3	Lascar	23° 18′59.84"S	67° 47′48.25"O	3890	Scoriae	Tumbres scoria flow[a]	–	9.2 Kyr

[a] Original name: "Tumbres Scoria Deposit: Flow deposit" in Gardeweg et al. (1998).
[b] Dome fragment emitted inside 1993 pyroclastic flow.

3.1.2. Gases

High-temperature (~260 °C) fumarole gases were collected on the northwestern flank of Lastarria during the 2014 IAVCEI CCVG (Commission on Chemistry of Volcanic Gases) 12th Volcanic Gas Workshop, whose aim was the inter-comparison of current gas sampling and measurements techniques among different groups of scientists (Lopez et al., 2018). Gases were sampled using a titanium tube inserted into the fumarole soil, then connected to a quartz line, with a silicone tube equipped with a three-way valve connected to a syringe for pumping the gas. Dry gases were finally stored in two-way Pyrex bottles of about 50 cc volume, with vacuum valves at both ends to prevent air contamination. To avoid any possible leak of helium from the bottles, noble gas analysis were carried out within two weeks from sampling date, which excludes any appreciable isotopic fractionation (e.g., Caracausi et al., 2005; Chiaradia et al., 2018). Further details of the sampling protocol can be found in Lopez et al. (2018).

3.2. Analytical techniques

3.2.1. Bulk-rock major and trace elements

Rock samples were prepared for analyzing major and trace elements in the DiSTeM laboratory at the University of Palermo. Bulk-rock analyses were performed at Activation Laboratories (Ancaster, Canada) following techniques described in i.e. Di Piazza et al. (2015) and Robidoux et al. (2017).

3.2.2. Mineral and glass chemistry

The mineral chemistry of the FIs-hosted minerals was studied using electron microprobe analysis (EMPA). For this purpose, sampled blocks, scoriae, and pumice fragments containing phenocrysts (Tables 1 and 2) were crushed and sieved several times until a homogeneous grain size of 0.5–1.0 mm was obtained. Several number of phenocrysts in this granulometric size range at Lascar ($n = 163$) and Lastarria ($n = 138$) were then characterized. Dense phenocrysts (>2.63 g/cm^3) were separated from scoriae, and less-dense minerals (e.g., plagioclase) were separated using sodium polytungstate liquid columns. The separated minerals were collected and washed with deionized water and acetone. The remaining scoriae and plagioclase samples were also stored and washed.

Mineral chemistry was analyzed at the HPHT (high-pressure/high-temperature) laboratory of Istituto Nazionale di Geofisica e Vulcanologia (INGV) in Rome using an electron microprobe analyzer (JXA-8200, JEOL) equipped with five wavelength-dispersive X-ray spectrometers and one energy-dispersive X-ray spectrometer analyzer. Plagioclases, olivines, Cpx, orthopyroxenes (Opx), and biotites were all prepared on different mounts after using abrasives and polishing down to 6-, 3-, and 1-μm diamond powder fractions. In Appendix I, augite duplicates spots on the same crystal were taken to verify reproducibility of results from major elements using the standard deviation (aug7552: 0.06–0.66 S.D.%). A set of reference crystals was used for quantifying each major element precision, which represents a relative standard deviation (S.D.) based on count-per-second (cps) (average Standard Error S.E. 0.313%). At least two spots on both the core and rim of each crystal were analyzed to identify composition changes during crystal growth (Appendixes I—V).

Matrix glass on the rim of separated phenocrysts and background (matrix) glass obtained from prepared thin sections were probed by EMPA. Glass surfaces from phenocrysts and closed inclusions with glassy texture were selected to study the chemical equilibrium in liquid–mineral and Opx–Cpx associations. For both glass and mineral surfaces, the EMPA conditions were a beam current of 7.50 nA, accelerating voltage of 15 kV, and beam diameter of 5 μm. The counting times for the minerals were 10 and 5 s at the peak and background, respectively.

3.2.3. Noble-gas element and isotope compositions

The concentrations and isotope compositions of noble gases (He, Ne, Ar) in fumarole gases and FIs were determined at the noble gas isotopic laboratory of INGV-Palermo. The laboratory is organized in function of the noble gas applications (elemental and isotopic analysis on solid and fluid matrices: https://www.pa.ingv.it/index.php/laboratorio-di-analisi-spettrometriche-per-gas-nobili/?lang=en) and consists of two rooms both equipped with purification lines and three mass spectrometers for the isotopic analysis of He, Ne, and Ar. Therefore, in the following subsections, we distinguish the description of laboratory protocols of samples preparation and analysis for fumarole gases and FIs.

3.2.3.1. Fumaroles. The ^{3}He, ^{4}He, and ^{20}Ne concentrations in fumarole gases were measured separately in a split-flight-tube mass spectrometer (GVI-Helix SFT, for analyzing the He isotopes) and in a multicollector mass spectrometer (Thermo-Helix MC Plus, for analyzing ^{20}Ne) after applying standard purification procedures (Batista Cruz et al., 2019; Di Piazza et al., 2015; Rizzo et al., 2015, 2016, 2019). The ^{3}He/^{4}He ratio is expressed in units of R/Ra (where Ra is the He-isotope ratio of air, 1.39×10^{-6}), and the analytical uncertainty (1σ) in single measurements was generally <0.3% (Table 3). The used standard was air, whose reproducibility across >50 analyses performed over several months was <3%. The ^{3}He/^{4}He ratios were corrected for atmospheric contamination using the measured ^{4}He/^{20}Ne ratio (e.g., Sano and Wakita, 1985) as follows:

$$Rc/Ra = ((RM/Ra)(He/Ne)_M - (He/Ne)_A)/((He/Ne)_M - (He/Ne)_A) \quad (1)$$

where subscripts M and A refer to measured and atmospheric values, respectively [$(He/Ne)_A = 0.318$]. The corrected ^{3}He/^{4}He ratios are reported in the main text and Table 3 as Rc/Ra values. The correction is small or negligible for most of the fumarole samples.

The Ar concentrations and isotope compositions (^{36}Ar, ^{38}Ar, and ^{40}Ar) were quantified in a multicollector mass spectrometer (Helix MC-GVI). The analytical uncertainty (1σ) for single ^{40}Ar/^{36}Ar measurements was <0.1%. The used standard was air, whose reproducibility over 1 year of daily analyses was <3.5%.^{40}Ar was corrected for air

Table 2
Chemical composition of bulk-rocks.

Sample	LAS1	LAS2	LAS3	LRA2	LRA3	LRA4
Volcano	Lascar	Lascar	Lascar	Lastarria	Lastarria	Lastarria
Material	Dome fragment	Scoriae Block	Scoriae Block	Scoriae Block	Pumice fragments	Pumice fragments
SiO_2 (wt%)	57.86	58.2	57.39	58.06	56.38	61.63
Al_2O_3	16.75	16.17	16.04	16.88	16.11	15.62
Fe_2O_3(T)	7.11	7.62	7.49	7.36	7.52	5.96
MnO	0.124	0.123	0.125	0.114	0.111	0.08
MgO	4.39	4.26	4.61	4.22	3.97	1.97
CaO	7.17	7.18	7.2	6.74	6.6	4.53
Na_2O	3.36	3.49	3.39	3.34	3.32	3.29
K_2O	1.61	1.57	1.54	1.95	2.36	3.03
TiO_2	0.724	0.821	0.776	0.979	1.02	0.907
P_2O_5	0.18	0.31	0.24	0.21	0.25	0.22
LOI	n.d.	0.3	0.14	0.7	2.27	2.22
Total	99.21	100	98.95	100.6	99.9	99.46
Sc (ppm)	21	18	20	14	15	9
Be	2	2	2	2	2	2
V	168	175	174	153	170	139
Ba	371	378	367	426	494	504
Sr	469	572	524	554	556	444
Y	19	20	19	15	18	16
Zr	127	142	135	177	190	205
Cr	110	100	90	170	110	90
Co	23	22	24	22	22	15
Ni	30	30	30	40	40	30
Cu	50	50	50	40	50	30
Zn	80	90	80	90	90	80
Ga	18	18	18	20	19	20
Ge	1	2	1	1	1	2
As	6	<5	<5	29	13	18
Rb	57	49	51	78	98	149
Nb	7	7	7	10	11	13
Mo	<2	3	<2	3	4	6
Ag	<0.5	<0.5	<0.5	<0.5	<0.5	0.7
In	<0.2	<0.2	<0.2	<0.2	<0.2	<0.2
Sn	2	2	1	2	2	2
Sb	1	0.9	1	2	1.1	1.5
Cs	3.5	2.8	3	5.1	6.7	11.6
La	19.5	22.9	20.7	29	37.6	39.3
Ce	40.3	46.8	43.1	60	77.5	81.5
Pr	4.74	5.71	5.2	7.04	9.05	9
Nd	19.2	22.7	20.5	26.5	33.3	34.5
Sm	4.1	4.7	4.2	5.2	6.1	6.1
Eu	1.04	1.16	1.16	1.29	1.45	1.3
Gd	3.7	4	3.9	4.1	4.7	4.4
Tb	0.6	0.6	0.6	0.6	0.7	0.7
Dy	3.4	3.8	3.5	3.1	3.7	3.5
Ho	0.7	0.7	0.7	0.5	0.7	0.6
Er	2	2.1	2	1.5	1.8	1.6
Tm	0.31	0.31	0.29	0.21	0.25	0.24
Yb	2	2	2	1.3	1.7	1.5
Lu	0.3	0.33	0.29	0.2	0.26	0.24
Hf	3	3.4	3.3	4.2	4.5	5.7
Ta	0.8	0.7	0.7	0.9	1	1.3
W	81	12	5	7	5	12
Tl	0.3	0.2	0.3	0.2	0.2	0.6
Pb	12	13	10	10	12	15
Bi	<0.4	<0.4	<0.4	<0.4	<0.4	<0.4
Th	6	5.7	5.6	14.6	19.1	29.9
U	2.2	1.8	1.9	4.4	5.7	9.2
La/Yb	9.8	11.5	10.4	22.3	22.1	26.2
Sc/Ni	0.7	0.6	0.7	0.4	0.4	0.3
$^*K_2O$/Yb	0.8	0.8	0.8	1.5	1.4	2.1
Ta/Yb	0.4	0.4	0.4	0.7	0.6	0.9
Y + Nb	26.0	27.0	26.0	25.0	29.0	29.0
$^*Na_2O + {}^*K_2O$	5.0	5.1	5.0	5.3	5.8	6.5
Mg#	55.0	52.6	55.0	53.2	51.1	39.6
$^*TiO_2$/100	4.0	4.6	4.3	5.4	5.8	5.2
Eu/Eu*=	0.80	0.80	0.86	0.82	0.80	0.73
Sr/Y	24.7	28.6	27.6	36.9	30.9	27.8
Ba/La	19.0	16.5	17.7	14.7	13.1	12.8
La/Sm	4.8	4.9	4.9	5.6	6.2	6.4
U/Th	0.4	0.3	0.3	0.3	0.3	0.3
Ba/Th	61.8	66.3	65.5	29.2	25.9	16.9

Bulk-rock major-element compositions were analyzed for major elements, trace elements, and REE using a combined ICP/MS device (WRA4B2) at Ancaster (Code 4B2-Std, Actlabs). Results of bulk-rock analyses of powder samples prepared at the DiSTeM laboratory at the University of Palermo. The measurement detection limits are also listed.

Table 3
Chemical and isotope compositions of noble gases in fumaroles from Lastarria.

Region	Locality	Lat.	Long.	Sample type	^{4}He ppm	^{4}He err.	^{20}Ne ppm	^{20}Ne err.	R/Ra	^{4}He/^{20}Ne	Rc/Ra	Error +/−	^{40}Ar ppm	^{40}Ar err.	^{36}Ar ppm	^{36}Ar err.	^{40}Ar/^{36}Ar	Error +/−	^{40}Ar[a]	^{4}He/^{40}Ar[a]	Ref.
Central Volcanic Zone	Lastarria CCVG3 lower fumarolic field	−25.154166	−68.523888	Dry gas samples from lower fumarole field	10.80	0.026	0.06	0.0007	5.34	176.76	5.35	0.048	75	0.006	0.239	8.73E-05	314.9	0.117	4.73	2.3	This work
Central Volcanic Zone	Lastarria CCVG2 lower fumarolic field	−25.154166	−68.523888	Dry gas samples from lower fumarole field	9.61	0.039	0.06	0.0007	5.27	157.37	5.28	0.050	n.a.	n.a.	n.a.	n.a.	n.a.	n.a.			This work
Central Andes Volcanic Zone	Lastarria	−25.154166	−68.523888	Lower fumarole field					5.13	159.9	5.14										Lopez et al. (2018)
Central Andes Volcanic Zone	Lastarria	−25.154166	−68.523888	Lower fumarole field					5.12	199.1	5.13										Lopez et al. (2018)
AIR					5.24		16.48		1	0.318			9278		31.4		295.5				AIR

[a] Sampling from site CCVG2 and CCVG3 at an altitude of ~5030 m a.s.l.

Table 4
Chemical and isotope compositions of noble gases in fluid inclusions of olivine and clinopyroxene.

Sample ID	Period of volcanism	Mineral	Weight	^{4}He	^{4}He Err.	^{20}Ne	^{20}Ne Err.	^{40}Ar	^{40}Ar Err.	^{36}Ar	^{36}Ar Err.	R/Ra	^{4}He/^{20}Ne	Rc/Ra	Err.	^{40}Ar/^{36}Ar	Err.	^{40}Ar*	^{4}He/^{40}Ar*
			g	mol/g	+/−	mol/g	+/−	mol/g	+/−	mol/g	+/−				+/−		%	mol/g	
LRA3	Lastarria: Ignimbrite 1–3	Cpx	0.84	6.6E-13	4.6E-16	2.4E-14	1.7E-16	4.8E-12	4.7E-15	1.6E-14	1.4E-16	6.53	27.4	6.60	0.07	308.1	0.04	2.0E-13	3.37
LRA3	Lastarria: Ignimbrite 1–3	Ol	0.12	3.1E-13	2.2E-15	5.6E-15	9.0E-17	3.8E-12	3.7E-14	1.2E-14	1.5E-16	7.97	55.4	8.01	0.18	303.5	0.13	9.9E-14	3.14
LRA2	Lastarria: Ignimbrite 3	Cpx	0.91	2.4E-14	5.0E-17	2.5E-14	3.8E-16	8.4E-12	1.0E-14	2.8E-14	1.5E-16	5.16	1.0	7.34	0.37	302.4	0.17	1.9E-13	0.12
LRA4	Lastarria: Ignimbrite 1	Cpx	0.69	1.6E-13	1.3E-16	2.1E-14	2.4E-16	2.4E-12	5.1E-15	7.3E-15	4.2E-17	5.11	7.6	5.31	0.10	307.2	0.04	2.1E-13	0.75
LAS1	Lascar: 1989, (Dome fragment, 1993)	Cpx	0.58	2.0E-13	1.8E-16	1.5E-14	1.7E-16	3.6E-12	1.3E-14	1.2E-14	5.0E-17	6.97	13.4	7.12	0.11	309.8	0.04	1.7E-13	1.19
LAS1 (xeno)[a]	Lascar: 1989, (Dome fragment, 1993)	Cpx	0.60	2.9E-13	1.9E-16	2.3E-14	3.6E-16	1.8E-12	6.2E-15	5.8E-15	2.7E-17	5.21	12.8	5.32	0.08	305.6	0.06	5.8E-14	4.98
LAS1 (xeno)[a]	Lascar: 1989, (Dome fragment, 1993)	Cpx	0.19	2.6E-13	1.8E-15	1.3E-15	2.2E-17	1.1E-12	1.1E-14	3.6E-15	4.4E-17	5.46	204.3	5.47	0.13	307.2	0.27	4.2E-14	6.06
LAS3	Tumbres scoria flow	Cpx	0.47	3.3E-13	3.2E-16	5.8E-14	8.8E-16	9.2E-12	3.3E-14	3.1E-14	1.4E-16	6.89	5.6	7.26	0.10	302.0	0.04	2.0E-13	1.64
LAS3	Tumbres scoria flow	Ol	0.09	2.5E-13	2.0E-15	1.1E-14	2.0E-16	7.5E-12	8.6E-14	2.5E-14	3.0E-16	6.82	21.7	6.91	0.24	300.2	0.08	1.2E-13	2.14

[a] Cpx xenocrystal of probable cumulitic origin. See text for more details.

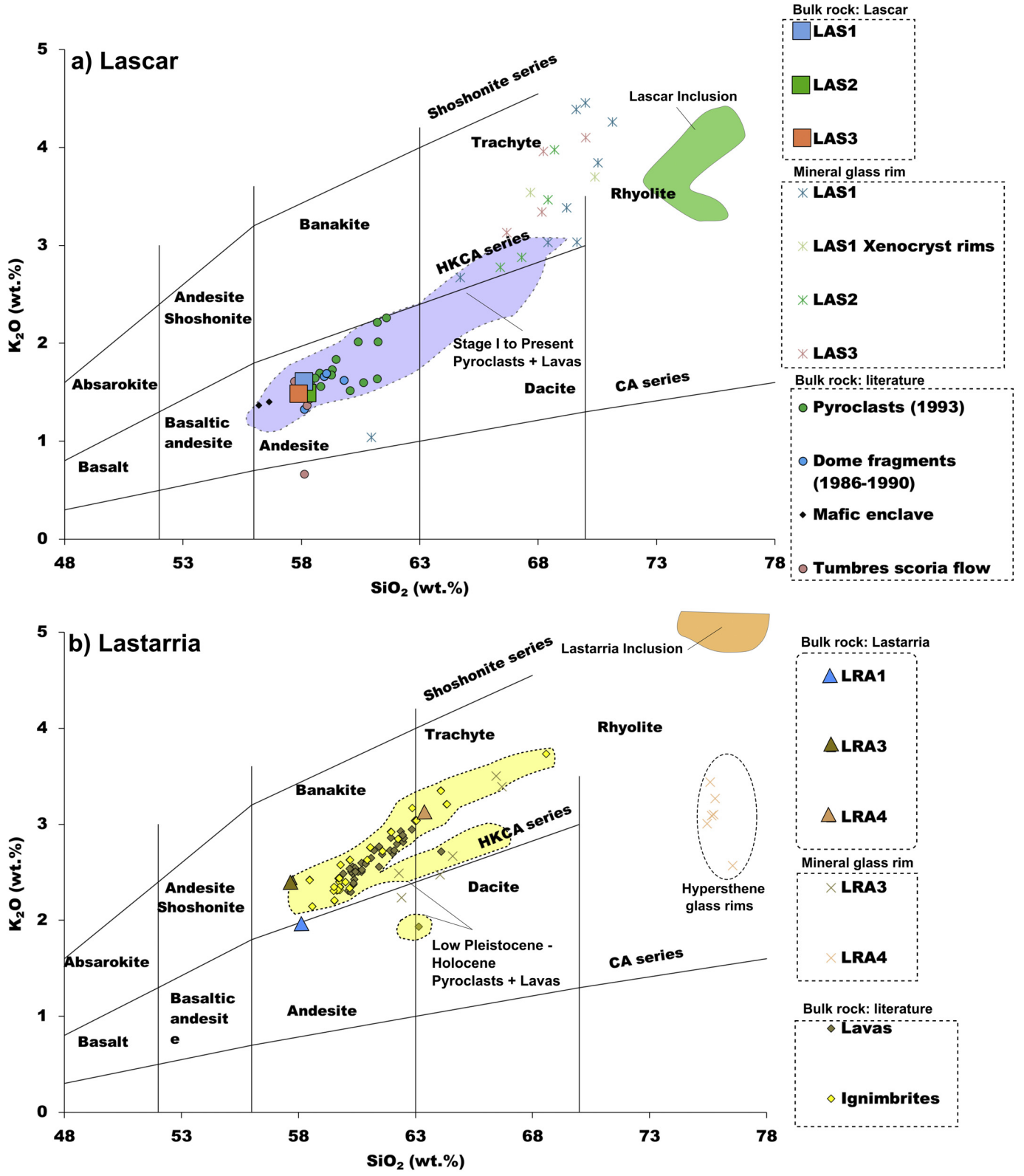

Fig. 2. Rock classification according to Peccerillo and Taylor (1977). Diagram of K_2O versus SiO_2 for bulk-rock compositions in this study and mineral glass rims and bulk-rock compositions in the literature. Compositional data are for (a) Lascar and (b) Lastarria. References for northern CVZ are listed in Scheinost (2018).

contamination ($^{40}Ar^*$) assuming that the ^{36}Ar present in our samples was derived from atmosphere, as follows:

$$^{40}Ar* = {}^{40}Ar_{sample} - \left(^{36}Ar_{sample} \times \left(^{40}Ar/^{36}Ar\right)_{air}\right)$$

Typical blanks for He, Ne, and Ar were $<10^{-15}$, $<10^{-16}$, and $<10^{-14}$ mol, respectively, and are at least two orders of magnitude lower than the sample signals at the relative mass spectrometers.

3.2.3.2. FIs in olivine and pyroxene crystals. The element and isotope compositions of He, Ne, and Ar were measured in FIs hosted in the olivine and pyroxene crystals at the noble gas isotopic laboratory of INGV-Palermo (Table 4). FIs are trapped as spherical or ellipsoidal gas or liquid bubbles during and after magma crystallization (Roedder, 1979, 1984). The olivine and pyroxene crystals studied in this work were separated from the same suite of samples investigated for the geochemistry of minerals and rocks within the fractions with sizes of 0.5–1 mm. The selected crystals were then cleaned and prepared for noble-gas measurements in accordance with a reproductible protocol (i.e. Battaglia et al., 2018; Boudoire et al., 2018; Di Piazza et al., 2015; Rizzo et al., 2015; Robidoux et al., 2017). Each group of samples (0.1–1.3 g) was then loaded into a six-position stainless-steel crusher. Noble gases trapped inside the FIs were released after in-vacuo single-step crushing, which minimizes the contribution of cosmogenic ^3He and radiogenic ^4He that could be trapped in the crystal lattice (e.g., Hilton et al., 2002; Kurz, 1986; Rizzo et al., 2015).

He isotopes (^3He and ^4He) and ^{20}Ne were measured separately by two different split-flight-tube mass spectrometers (Helix SFT-Thermo). The analytical uncertainty (1σ) of the He-isotope ratio measurements was <5%. The used standard was air, whose reproducibility across >20 analyses performed over several months was <2%.

Ar isotopes (^{36}Ar, ^{38}Ar, and ^{40}Ar) were analyzed by a multicollector mass spectrometer (GVI Argus) at an analytical uncertainty (1σ) of <0.4%. The used standard was air, whose reproducibility across analyses performed over >2 years was <1%.

The correction of $^3He/^4He$ ratios (Rc/Ra) is small (maximum bias of ~0.2 Ra) or negligible for most of the samples, except for Cpx from LAS3 and LRA2 where it exceeds 0.2 Ra due to $^4He/^{20}Ne$ values <6 (Table 4).

Typical blanks for He, Ne, and Ar were $<10^{-15}$, $<10^{-16}$ and $<10^{-14}$ mol, respectively, and were at least one order of magnitude lower than the values measured in the samples. Further details about the sample preparation and analytical procedures are available in Di Piazza et al. (2015), Rizzo et al. (2015, 2018), Robidoux et al. (2017), Battaglia et al. (2018), and Faccini et al. (2020).

4. Results

4.1. Bulk-rock geochemistry

4.1.1. Lascar volcano

The major-element compositions of bulk-rock samples are presented in Table 2. Our Lascar rock samples are andesitic (Fig. 2a) and fairly homogeneous (SiO_2 = 58.1–58.3 wt%, K_2O = 1.56–1.62 wt%, MgO = 4.26–4.61 wt%), and thus overlap with the compositions of the least-differentiated Lascar mafic enclaves, Tumbres scoria flow and the least differentiated 1993s eruption products (e.g., Gardeweg et al., 2011; Matthews et al., 1994, 1999). The bulk-rock composition range for Lascar is wider in the published literature, ranging from andesitic to dacitic (SiO_2 < 56.6–69.4 wt%, K_2O = 1.3–3.8 wt%) and falling within the fields of CA and HK-CA series (Deruelle, 1982; Mamani et al., 2010; Matthews et al., 1994, 1999; Menard et al., 2014) (Fig. 2a).

Lascar trace-element rock compositions exhibit La/Yb of 9.8–11.5 and Sc/Ni of 0.6–0.7. Sr/Y varies in a narrow range 24.7–28.6 (Table 2). The Eu anomaly is small and constant (Eu/Eu^* = 0.80–0.86). Lascar rocks are slightly enriched in large-ion lithophile elements (e.g., Cs, Rb, Sr, and Ba) relative to N-MORB, and they overlap with *E*-MORB. Most samples have low contents of the high-field-strength elements (HFSE) Ta, Nb, Zr, and Hf. Ba/La, U/Th, and Ba/Th values, which indicate sediments and fluids components from subducting slab, are 16.5–19, 0.3–0.4, and 61.8–66.3, respectively. La/Sm is 4.8–4.9 (Table 2).

4.1.2. Lastarria volcano

Fig. 2b plots the bulk-rock compositions of our Lastarria samples in the context of the results obtained in previously reported studies. Our samples are intermediate to felsic (SiO_2 = 58.2–63.4 wt%, K_2O = 2.0–3.1 wt%, MgO = 1.97–4.22 wt%) (Table 2), and fall within the same HK-CA series evolutionary trend (Mamani et al., 2010) defined by bulk-rock literature data (SiO_2 = 58.6–69.4 wt%, K_2O = 2.0–3.8 wt%; Naranjo, 1992; Wittenbrink, 1997; Naranjo, 2010; Stechern et al., 2017) (Fig. 2b). LRA3 and LRA2 are among the least-differentiated Lastarria rocks (Naranjo, 1992), while sample LRA4 (taken from Ignimbrite 1 emitted by crater 3) is more evolved (SiO_2 = 63.4 wt%). LRA4, although evolved, has a lower silica content than the most-differentiated Lastarria group of samples: the Negriales lava field (Naranjo, 1992; Fig. 2b). Overall, rocks LRA2, LRA3, and LRA4 are alkali-rich (>5.3 wt%) and have low Mg# values (Mg/(Mg + Fe) <53.0%.

Trace elements in Lastarria rocks show high La/Yb values (22.1–26.2), low Sc/Ni (0.3–0.4), small Eu anomalies (Eu/Eu^* = 0.73–0.82), and are richer in large-ion lithophile elements (e.g., Cs, Rb, Sr, and Ba) compared with Lascar. Sr/Y varies from 27.8 to 36.9 (Table 2). Most samples have low contents of HFSE, but the concentrations are slightly higher than those at Lascar (Table 2). For tracing subduction fluid signal, the Lastarria rocks exhibit low Ba/La (12.8–14.7), U/Th (0.3), and Ba/Th (16.9–29.2). La/Sm is 5.6–6.4 (Table 2).

4.2. Petrography and mineral chemistry

4.2.1. Lascar volcano

The phenocryst concentration decreases in the following order at Lascar: plagioclase > Cpx > Opx > olivine > magnetite. Dome fragments (LAS1) are nonvesicular and densely microporphyric. Scoriae fragments (LAS1 and LAS2) with sizes from lapilli to bomb are all porphyric, but they exhibit various degrees of vesicularity. The LAS1 xenocrystals represent a coarse granulate cumulate of Cpx-plagioclase assemblage found in the dome fragment. The major-element concentrations from those Cpx-plagioclase minerals forming the granular cumulate are compared with the rest of the Cpx and plagioclase found as dispersed porphyric mineral phases in Figs. 3 and 4. The full results obtained in the mineral chemistry analyses of Lascar and Lastarria samples are reported in Appendixes II–V and illustrated in Fig. 3.

The LAS1 dome fragments mainly contain porphyric plagioclases (An_{32-60}) and green Cpx here identified as augite species ($Wo_{39-46}En_{38-50}Fs_{8-14}$) with moderate Mg# values (Mg/(Mg + Fe) = 72–86%, average 81%; Fig. 3c) (e.g., Linsley, 1983). Three of seven core–rim Cpx pairs show normal zoning, but the rest have homogeneous compositions (Fig. 3c). In the dome fragments (LAS1), pyroxenes-plagioclase granular cumulates are found with similar compositions to phenocrysts of augite and plagioclase sampled in the rest of the rock fragments ($Wo_{39-49}En_{40-53}Fs_{5-17}$ with Mg# = 72–87% and 80 ± 5%) (An_{46-70}). One distinction is that the plagioclases in cumulates are rather heterogeneous with Na content, with few crystals reaching consistency with the andesine group (Fig. 3f, Appendix IV).

The LAS2 dark scoriae fragments from the eruption of 1993 present three of six samples of augite phenocrysts with normal zoning, while five LAS3 core–rim pairs have reverse zoning in Tumbres scoria flow, five have normal zoning, and one is homogeneous. The greenish Cpx found in LAS3 (augite; $Wo_{40-56}En_{41-52}Fs_{6-15}$) have moderate Mg# values (81 ± 5%) and compositions similar to that of LAS2 (Fig. 3c). Matthews et al. (1994) reported that 1993 scoriae and pumice exhibit lower Mg# values of 73–78% and 73–82%, respectively.

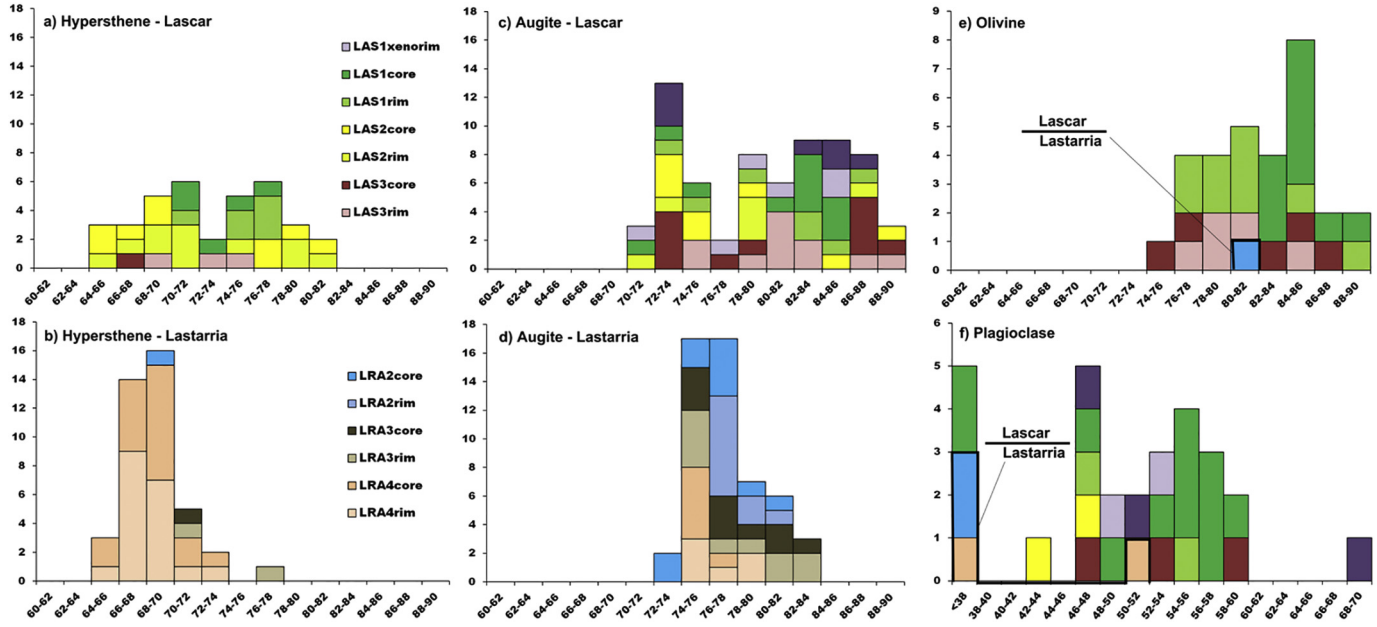

Fig. 3. Frequency diagrams of Mg#. Core and rim Mg# values provided for each crystal in the studied rock samples from Lascar (LAS1, LAS2, and LAS3) and Lastarria (LRA2, LRA3, and LRA4). (a) Hypersthene from Lascar, (b) hypersthene from Lastarria, (c) augite from Lascar, (d) augite from Lastarria, (e) olivine from Lascar and Lastarria, and (f) plagioclase An# contents from Lascar and Lastarria.

The LAS2 scoriae fragments have $An_{43–47}$ plagioclases and abundant green Cpx (augite; $Wo_{40–45}En_{39–50}Fs_{6–16}$) with moderate Mg# values (73–90%, 78 ± 6%). In comparison, the LAS3 older scoriae fragments contain labradorites ($An_{47–58}$).

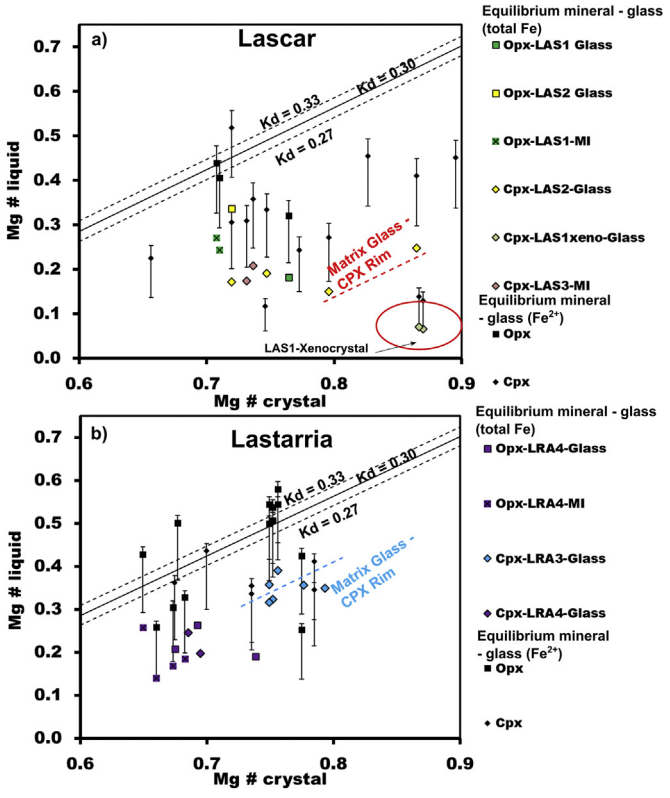

Fig. 4. Crystal versus liquid compositions. Mg# values for liquid (glass) are compared to Mg# values for minerals (hypersthenes and augite are indicated by colored squares and lozenges, respectively). Equilibrium mineral–glass (total Fe) values are plotted along with data from the literature. The results indicate Fe^{2+} (fully black symbols: hypersthenes and augites are indicated by squares and lozenges, respectively). Data are for (a) Lascar and (b) Lastarria.

Opx minerals are less abundant (Fig. 3a), with hypersthenes as the dominant species. Sample LAS1 from dome fragments contains hypersthenes ($Wo_{2–4}En_{68–70}Fs_{20–29}$) with moderate Mg# values (71–78%, 75 ± 3%). The hypersthene core–rim pairs have Mg# values similar to those of the 1986–1993 Lascar dome samples (~69–77%) reported by Matthews et al. (1994). The hypersthenes from LAS2 scoriae show wide Mg# ranges (65–81%). LAS3 scoriae hypersthenes have similar compositions ($Wo_{2–3}En_{64–83}Fs_{13–33}$) with moderate Mg# values (67–86%, 75 ± 6%) and thus are similar to the crystals of 1993 scoriae. The Mg# values increase moderately from the core to the rim (Fig. 3a).

The olivines in dome samples were abundant and primitive ($Fo_{77–90}$, $Fo_{83±4\%}$; Fig. 3e). Olivines were not analyzed in the LAS2 scoriae and can only be observed under a microscope. The olivines in older scoriae (LAS3) are abundant and slightly less primitive ($Fo_{76–86}$, $Fo_{80±4\%}$; Fig. 3e). Only 1 of 15 olivines show reverse zoning, while six clearly show forsterite contents decreasing from the core to the rim (Fig. 3e).

4.2.2. Lastarria volcano

Scoriae and pumice blocks have distinct phenocryst assemblages at Lastarria, with a porphyritic texture and a wide range of microphenocryst (void-free) concentrations in the LRA2, LRA3, and LRA4 samples. The phenocryst concentration decreases in the following order: plagioclase > Cpx > Opx > biotite > hornblende (trace) > magnetite. Very few olivine crystals were observed as phenocrysts. Scoriae fragments with sizes ranging from lapilli to bombs are highly vesicular (small pores), and the groundmass is generally microcrystalline to glassy. Pumices have various colors and show signs of mingling, with frequent interconnections between clear and dark bands (e.g., Naranjo, 1992; Stechern et al., 2017).

The mineral assemblage indicates differentiated magmas at Lastarria (olivine, Fo_{82}; augite, $Wo_{38–44}En_{41–48}Fs_{9–14}$; hypersthene, $Wo_{1–3}En_{62–70}Fs_{23–35}$; plagioclase, $An_{38–52}$). Substantial compositional dissimilarities exist between different LRA1, LRA2, LRA3, and LRA4 samples (Fig. 3d). Amphiboles and apatites are found also as phenocrysts with spinel/magnetite inclusions and intergrowth (see Stechern et al., 2017).

The LRA2 scoriae blocks contain high concentrations of porphyric plagioclases ($An_{22–26}$), while plagioclases in pumice fragments from LRA4 appear more evolved ($An_{37–52}$). Few plagioclases were analyzed overall ($n = 6$). Stechern et al. (2017) classified plagioclases as

labradorite and andesine, similarly to the present study (Fig. 3f, Appendix IV).

Scoriae LRA2 samples contain Cpx identified as augite species ($Wo_{39-44}En_{42-48}Fs_{11-15}$) with moderate Mg# values (73–81%, 77 ± 2%; Fig. 3d). The augites are slightly more primitive in LRA3 pumices ($Wo_{40-45}En_{41-48}Fs_{9-15}$ with Mg# = 75–84%) than LRA4 ($Wo_{42-44}En_{42-45}Fs_{12-15}$ with Mg# = 75–79%). For core–rim pairs in LRA2, three of nine phenocrysts exhibit reverse zoning while the rest are homogeneous. In LRA3, 10 core–rim pairs comprise 4 with reverse zoning, 3 with normal zoning, and 3 that are homogeneous. In LRA4, three of six phenocrysts exhibit reverse zoning while the rest are homogeneous.

In LRA2, Opx were analyzed and identified as hypersthene species ($Wo_{1-3}En_{73-83}Fs_{14-24}$; Mg# = 70%). In pumice fragments from LRA3 fragments, hypersthenes are found as intergrowth Cpx-Opx crystals ($Wo_3En_{83}Fs_{14}$; Mg# = 70–86%), whereas augites are more differentiated ($Wo_{2,3}En_{73-74}Fs_{22-24}$; Mg# = 75–84%). In LRA4, pumice fragments contain hypersthenes ($Wo_{2,3}En_{67-74}Fs_{25-33}$) with moderate Mg# values (75–78%). Zoning does not appear frequently (being observed in only 6 of 21 samples, mostly in LRA4), among which 3 show clear reverse zoning.

Micas are frequent in pumice fragments and include several large glass inclusions, but many contain plagioclase and pyroxene solid inclusions. The Fe contents estimated from stoichiometric calculations (Howie et al., 1992) indicate that most micas have Fe/(Fe + Mg) ratios of 0.28–0.32 (Appendix V). Those ratios are thus close to the phlogopite–biotite transition (Fe/(Fe + Mg) = 0.33). Micas have Si/$Al^{(IV)}$ ratios of 2.40–2.48.

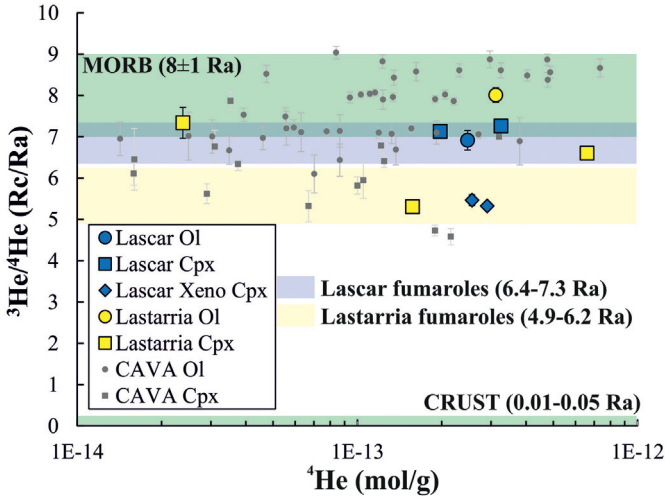

Fig. 5. ^4He concentration (mol/g) versus $^3He/^4He$ ratios corrected for atmospheric contamination (Rc/Ra) in FIs. The $^3He/^4He$ ranges of MORB (8 ± 1 Ra; Graham, 2002) and Crust (0.01–0.05 Ra; Ozima and Podosek, 2002) are reported as green bars. The yellow and blue bars indicate the ranges of $^3He/^4He$ measured in Lastarria and Lascar fumaroles that include our (for Lastarria only) and literature data (Aguilera et al., 2012; Lopez et al., 2018; Tassi et al., 2011). Fis data from CAVA (Central American Volcanic Arc) includes $^3He/^4He$ values from Turrialba, Irazu, Cerro Negro, Nejapa, San Cristobal, and Pacaya volcanoes (Shaw et al., 2006 and references therein; Di Piazza et al., 2015; Robidoux et al., 2017; Battaglia et al., 2018). (For interpretation of the references to colour in this figure legend, the reader is referred to the web version of this article.)

4.3. Glass inclusions and matrix glass compositions

4.3.1. Lascar volcano

Matrix glasses around phenocrysts were probed to verify mineral–liquid equilibrium (Appendix VI). Spherical and ellipsoidal glass inclusions were also observed and analyzed, but the differentiated nature of those inclusions (SiO_2 = 73.8–76.8 wt%, K_2O = 3.5–4.2 wt%; Fig. 2a) made it difficult to use them for barometry calculations (see below). Most hypersthene and augite euhedral crystals have fully enclosed glassy inclusions without postentrapment characteristics, so their major-element compositions are likely to be unaffected by elemental diffusion in crystal hosts (Danyushevsky et al., 2004). The crystal host compositions are listed in Appendix VII.

Lascar matrix glasses are andesitic to trachytic and follow steep K-versus-Si evolution trends (Fig. 2a; SiO_2 = 61.0–72.1 wt%, K_2O = 1.0–5.1 wt%). The most-primitive glasses are found around hypersthene minerals from dome fragments (SiO_2 = 61.0–70.0 wt%, K_2O = 1.0–4.5 wt%, Mg# ≤ 36%), while most Cpx and plagioclase glass rims are trachytic to rhyolitic. Fig. 4a demonstrates that magnesium distribution coefficients measured from sets of mineral–glass couples are below olivine ($Kd_{Fe\text{-}Mg}$ = 0.30 ± 0.03) or Cpx ($Kd_{Fe\text{-}Mg}$ = 0.27 ± 0.03) equilibrium values, with a few exceptions. The Cpx-plagioclase cumulates contrast the most from the mineral–liquid Kd being in equilibrium (Fig. 4a), and so they were considered as xenocrysts in this study.

4.3.2. Lastarria volcano

Lastarria matrix glasses exhibit andesitic, banakitic, and trachytic compositions (SiO_2 = 62.3–76.6 wt%) and are particularly rich in K (K_2O = 2.3–5.6 wt%). Hypersthene glass rims exceptionally show evolved rhyolitic compositions (SiO_2 > 75.5 wt%, K_2O > 5.0 wt%, Mg# < 26.3%), and are richer in alkalis compared with Lascar (Fig. 2b, Appendix VI).

Spherical and ellipsoidal glass inclusions are also rather evolved (SiO_2 = 53.7–75.9 wt%, K_2O = 0.6–6.0 wt%). Opx, Cpx, and biotite crystals have fully enclosed glass inclusions without postentrapment characteristics. The crystal host compositions are listed in Appendix VII, and the mineral host compositions from biotite are listed in Appendix V.

Distribution coefficients for Fe are closer to equilibrium values than for the Lascar samples (Fig. 4). In total, two inclusions and three glasses cross the equilibrium lines within the margin of error. Equilibrium is reached for those samples with maximum Fe^{3+}/Fe^{2+} ratios (1.16 ± 0.16) and minimum Mg# values.

4.4. Element and isotope compositions of noble gases

4.4.1. Fumaroles

Two dry gases were collected from a single high-temperature (about 260 °C) fumarole on the lower field at the base of Lastarria cone (5030 m a.s.l.). The two samples yielded reproducible results (for He and Ne; Ar was analyzed in only one sample), which are presented in Table 3. In detail, the He concentrations were 9.6 ± 0.04 and 10.8 ± 0.03 ppm, while the Ne concentration was 0.06 ± 0.0007 ppm in both samples (the corresponding $^4He/^{20}Ne$ ratios are 157.4 and 176.8). These results are comparable to those reported by Lopez et al. (2018) for samples obtained during the same sampling campaign. The ^{40}Ar concentration was 75 ± 0.06 ppm, with a $^{40}Ar/^{36}Ar$ ratio of 315 ± 0.12 (Table 3). $^4He/^{20}Ne$ and $^{40}Ar/^{36}Ar$ indicate the presence of moderate-to-severe air contamination, since the $^{40}Ar/^{36}Ar$ ratio remains slightly above the theoretical ratio in atmosphere ($^{40}Ar/^{36}Ar$ = 295.5; Ozima and Podosek, 2002). $^{40}Ar^*$ corrected for air contamination was calculated in the only sample were Ar isotopic analysis was carried out and yields 4.7 ppm, with a corresponding $^4He/^{40}Ar^*$ of 2.3 (Table 3).

The Rc/Ra values are 5.28 ± 0.05 Ra and 5.35 ± 0.05 Ra (Figs. 5 and 6).

Fumaroles at Lascar volcano were not sampled in this study, and so below we only consider literature data for comparison with our measures in FIs.

4.4.2. Fluid inclusions

The concentrations and isotope ratios of noble gases in FIs and relative analytical uncertainties are reported in Table 4. The LAS3 rock was the only one from Lascar volcano where it was possible to hand pick sufficient (~0.1 g) olivines for measuring noble gases. The resulting noble-gas concentrations were 2.5 × 10^{-13} mol/g for He (Fig. 5), 1.1 × 10^{-14}

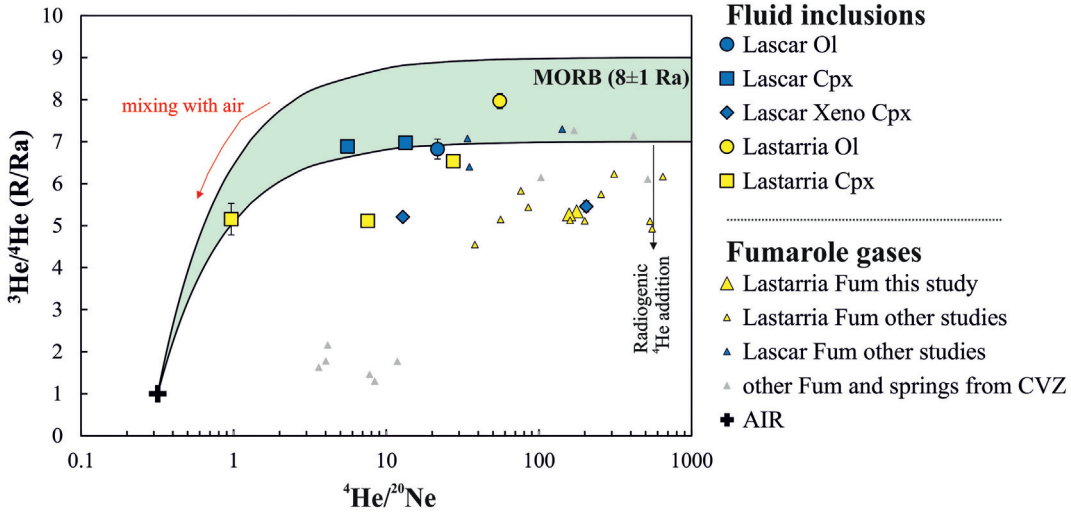

Fig. 6. $^{4}He/^{20}Ne$ versus $^{3}He/^{4}He$ (R/Ra) in FIs and fumaroles. Literature data of fumarole gases from Lascar, Lastarria and other geothermal and volcanic areas from CVZ are from Hilton et al. (1993), Tassi et al. (2009, 2011), Aguilera et al. (2012), and Lopez et al. (2018).

mol/g for Ne, and 7.4×10^{-12} mol/g for Ar (Table 4). Cpx from the same sample showed a comparable amount of He (3.3×10^{-13} mol/g; Fig. 5) but higher Ne and Ar contents (5.8×10^{-14} and 9.2×10^{-12} mol/g, respectively), thus indicating greater air contamination. FIs from LAS1 Cpx phenocrystals displayed He, Ne, and Ar concentrations of 2.0×10^{-13}, 1.5×10^{-14}, and 3.6×10^{-12} mol/g, respectively (Fig. 5). FIs from LAS1 Cpx xenocrystals from cumulates (see Section 4.3.1) displayed He, Ne, and Ar ranges of concentrations of $2.6–2.9 \times 10^{-13}$, $1.2–22.7 \times 10^{-15}$, and $1.1–1.8 \times 10^{-12}$ mol/g, respectively (Fig. 5).

Among Lastarria samples, only in LRA3 it was possible to hand pick sufficient olivines for measuring noble gases; the other samples were analyzed for Cpx only. The He, Ne, and Ar concentrations in olivine FIs were 3.1×10^{-13}, 5.6×10^{-15}, and 3.8×10^{-12} mol/g, respectively (Fig. 5, Table 4). FIs from Cpx in LRA2, LRA3, and LRA4 yielded He, Ne, and Ar concentrations of $0.2–6.6 \times 10^{-13}$, $2.1–2.5 \times 10^{-14}$, and $2.4–4.8 \times 10^{-12}$ mol/g, respectively (Fig. 5, Table 4).

The $^{4}He/^{20}Ne$ and $^{40}Ar/^{36}Ar$ ratios had ranges of 5.6–204.3 (Fig. 6) and 300–310, respectively, in Lascar samples, and of 1.0–55.4 (Fig. 6) and 302–308 in Lastarria samples.

$^{40}Ar^{*}$ varies between 9.9×10^{-14} and 2.1×10^{-13} mol/g, with a corresponding $^{4}He/^{40}Ar^{*}$ between 0.1 and 3.4 (Table 4).

The Rc/Ra values vary between 6.9 ± 0.24 Ra and 7.3 ± 0.10 Ra in olivines and Cpx from LAS1 and LAS3, while they are lower (5.3 ± 0.08 Ra and 5.5 ± 0.13 Ra) in LAS1 Cpx xenocrysts (Fig. 5). Among Lastarria samples, the Rc/Ra values vary between 5.3 ± 0.10 Ra and 8.0 ± 0.18 Ra (Fig. 5). The ratio was highest for LRA3 olivines and lowest for LRA4 Cpx (Table 4). It should be noted that a strong atmospheric correction was found for LRA2 Cpx ($^{4}He/^{20}Ne = 1.0$), with a marked difference between R/Ra and Rc/Ra (2.2. Ra of bias). This sample has the lowest He content (2.4×10^{-14} mol/g) and the lowest $^{4}He/^{40}Ar^{*}$ (0.1; see Section 5.2), which could indicate a preferential diffusive loss of He from the crystal (e.g., Burnard, 2004; Faccini et al., 2020; Rizzo et al., 2018). Due to this possible secondary effect, we ignore this sample in the discussion below (see Table 4).

5. Discussion

5.1. Geothermobarometry of the plumbing system

We initially used pairs of mineral–liquid compositions to estimate the pressure/temperature (P/T) conditions of crystallizing magmas under the Lascar and Lastarria volcanoes. To achieve this aim we utilized major oxide concentrations as input parameters in different mineral–liquid equilibrium geothermobarometers (see Appendixes VI and VIII). To obtain a maximum estimate for pressures and temperatures of magma storage, results are discussed regarding saturated hydrous melt conditions (Appendix IX, X). Three mineral–liquid thermobarometer data sets were obtained for Cpx-Opx, clinopyroxene–liquid (Cpx-L), and orthopyroxene–liquid (Opx-L) pairs based on the model of calculation from Putirka (2008) (Appendix VIII).

5.1.1. Lascar volcano

Three sequences of volcanic events triggered by recharges of mafic magma were modeled for estimating their maximum ranges of P/T conditions at Lascar since ~9.2 ky (Gardeweg et al., 1998); the 1993´s Sub-Plinian period (LAS2), the 1986–1993´s previous dome building cycle (LAS1) and the Tumbres scoriae flow (LAS3). As observed in the P/T diagram (Fig. 7a; Appendix VIII), we assume those magmas have been ascending in the crust following an isothermal decompression phase and a decompression/extended cooling phase. These two-steps of magma decompression represent all sampled products (LAS1, LAS2, and LAS3) that crystallized with a two-pyroxene equilibrium for different storage zones and covering a depth of at least 41 km in the lithosphere (Fig. 7a).

In detail, the Cpx-Opx thermobarometer and mineral chemistry data indicate hypersthene and augite species at Lascar with compositions that are consistent with thermodynamic equilibrium at 642–649 MPa and 1079–1092 °C (Fig. 7a, Appendixes VI and VIII). The Cpx-L temperatures for Lascar are correlated with the pressure changes ranging from 1094 to 1181 °C (1108 ± 32 °C, $n = 11$), while the range of Opx-L temperatures is 875–1023 °C (913 ± 70 °C, $n = 5$).

The Cpx-L pair are in equilibrium for LAS1 output pressures between 305 and 546 MPa, except for LAS1 augite xenocrysts that are chemically far from the Kd equilibrium and farther than the other mineral–liquid Mg# pairs (Fig. 4a). Phenocrysts and xenocrysts both record core-rim chemistry variations slightly normal or, in few cases, inverse, without extreme changes in compositions as they grow external rims (only ~10% of Cpx Mg#) (Fig. 3c). Evidences that larger xenocrysts of augites-plagioclases are crystallized prior to the group of single phenocrysts are testified via Anorthite heterogeneities and the presence of inverse zoning in plagioclases (Fig. 3f, Appendix IV). A certain hiatus in primitive augite nucleation would explain differences in mineral chemistry (Cpx Mg# > 87%; Fig. 4a) (Marsh, 1998), or perhaps the LAS1 xenocrysts represent older unequilibrated crystals (glomerocrysts) transported in ascending liquids with variable levels of differentiation (liquid Mg# < 10%; Fig. 4a) (Marsh, 1998, 2013).

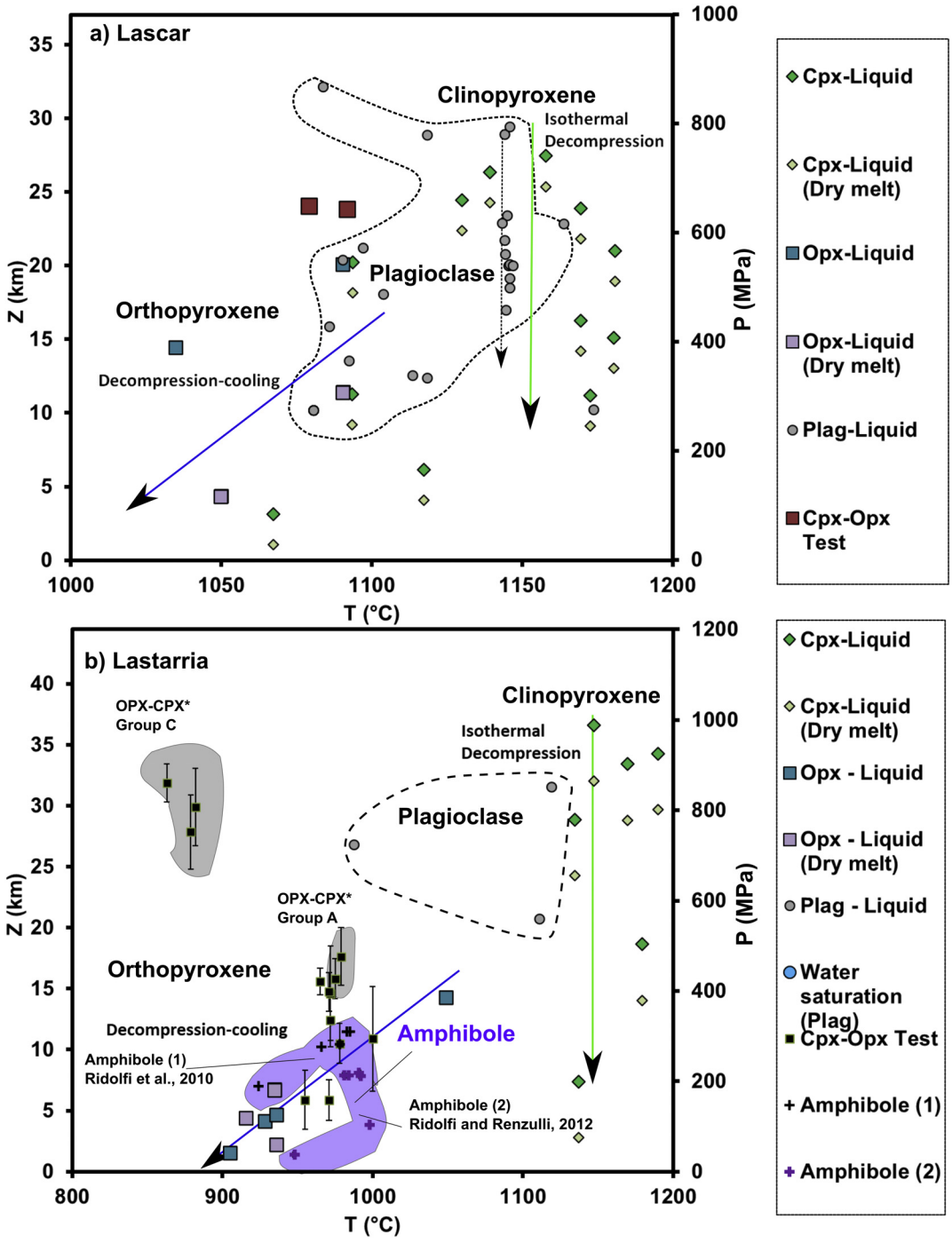

Fig. 7. Geobarometers. Graphs of estimated P/T relationship for magma crystallization conditions (lithostatic pressure gradient is 27 MPa/km). The geobarometers include Opx-L and Cpx-L pairs from Putirka et al. (2003) and eq. 32c in Putirka (2005) are plotted for Lascar and Lastarria data sets. The Cpx-Opx thermobarometer data are compared when mineral pairs are observed in rock samples (eqs. 38 and 39 in Putirka, 2008). Data sets for plagioclase-liquid pairs (Lange et al., 2009) are illustrated with water contents of the liquid melt system listed in Appendix VI and VII. Cpx and Opx versus liquid equilibrium geobarometers are estimated in dry and wet conditions (Putirka, 2005, 2008). Amphibole pressures and temperatures from Stechern et al. (2017) were obtained using Ridolfi et al. (2010) for amphibole (1) data, and Ridolfi and Renzulli (2012) for amphibole (2) models. Data are for (a) Lascar and (b) Lastarria.

LAS1 hypersthene pressures (Opx-L) reach 542 MPa (Fig. 7a), similar to augites (546 MPa). This is likely to correspond to maximum pressure conditions since none of these crystals have their rim composition in equilibrium with the surrounding glass (Appendix VIII). In LAS3, we infer pressures between 166 and 660 MPa for augite equilibrium, and its association with hypersthenes (as trapped solid inclusions) indicate that intergrowth of the two phases is possible under equilibrium conditions (Fig. 7a). For hypersthene and augite, we find an overall improved Mg# equilibrium between the glass rim versus phenocryst rim compositions (Fig. 4a). Consequently, the crystallization sequence implies equilibrium of mafic minerals (Cpx or Opx) with the surrounding melts at depth between 4 and 22 km (Fig. 7).

Based on those results and the evolution of P/T parameters, we propose the existence of an area with deep mafic magma reservoirs that would represent the ranges of lithostatic pressure depths shown in Fig. 10a (~ 660 MPa). Lower pressure values (<305 MPa) would

represent the decompression cooling phase of the same ascending magma body with increasing plagioclase crystallization (see Fig. 4a). This is likely to occur at shallower levels, possibly corresponding to the pounding zone illustrated in Fig. 10a.

Some peculiarities persist in the most-recent samples (LAS1, LAS2), which complicate modeling of the historic to present magmas to the same Liquid Line of Descent (LLD). To this regard, the mineral relative magnesium content (Mg# for olivine, hypersthenes, and augite) and glass compositions at Lascar from the 1986–1993 collapse of dome growth (LAS1) is associated to a magma being slightly more differentiated than for the 1993 explosive sequence (LAS2) (Fig. 2a, Fig. 3a–c, Fig. 4a). As discussed previously, crystals of dome growth also show Mg# heterogeneities in their magma components, as evidenced by bimodal mafic mineral values and unequilibrated Kd values (Fig. 3a). The dome fragments thus could represent a fractionated magmatic phase presumably with faster crystallization rates (Marsh, 1998). The emitted scoriae (LAS2) present in the pyroclastic flow of the 1993 eruption represents instead a direct and fast magmatic ascent which is passing the previous magma batches (i.e. *bypassing* the differentiated magma; Matthews et al., 1999).

Uncertainty still remains about the origin of trachitic-to-rhyolitic glass compositions probed on the mineral–glass pairs of our Lascar samples (SiO_2 = 72–73 wt%; Fig. 2a) as no textural evidence of mixing have been observed on the rock fragments (except Tumbres scoriae flow; Matthews et al. 1994). Such differentiated products have already been reported for emissions from the central crater and eastern vents of Lascar (Gardeweg et al., 2011; Matthews et al., 1999). In addition, white pumices with felsic compositions were found in the lithic-rich and pumice-rich lenses of the 1993 pyroclastic deposits (Calder et al., 2000; Sparks et al., 1997). The presence of overlapping levels of melt differentiation makes complex LLD modeling to a single parental melt (i.e. Cashman and Edmonds, 2019), even for the most recent magmatic recharges illustrated in our Fig. 10a. Consequently, the mafic magmas emitted during the 1986–1993 dome building phase and sub-plinian 1993s eruptive sequences are susceptible to follow distinct cooling-decompression paths inside the crust (305–660 MPa) even if they spatially coincide in shallow reservoirs (Fig. 10a).

5.1.2. Lastarria volcano

The three mineral–liquid thermobarometer data sets show that cooling/decompression behaviors affect Lastarria as they do Lascar (Fig. 7, Appendix VIII). Based on those results and the evolution of P/T parameters, we derived an equivalent lithostatic pressure model for the magmas that produced Ignimbrites since ~4.85 ky A.P. (Fig. 10a). The most-recent Ignimbrite 3 (which is younger than ~2.46 ky) did not have mineral–liquid $Kd_{Fe\text{-}Mg}$ in equilibrium in our samples, and so its thermodynamic condition parameters were based on the data of Stechern et al. (2017). No equilibrium pressures were encountered for LRA1 and LRA2, which were associated with Group C in Stechern et al. (2017) that corresponds to a source at a depth of ~20–40 km.

The detailed P/T data show hydrous Cpx-L pressures that are particularly variable at Lastarria, ranging from 989 MPa down to 503 MPa, with $Kd_{Fe\text{-}Mg}$ being in equilibrium (Fig. 7b, Appendix VIII). Hypersthenes are in equilibrium from 386 MPa down to <112 MPa at Lastarria. At Lastarria the Cpx-L temperatures are 1135–1190 °C (1140 ± 38 °C, n = 5), while those of Opx-L are 904–935 °C (921 ± 13 °C, n = 6). Many results for the tested Cpx-L and Plagioclase (Pgl)-L thermobarometric pairs follow vertical pressure decreases for relatively constant temperatures (isothermal decompression; Fig. 7b, Appendix VIII, IX).

Mineral chemistry analyses from hypersthene, augite, and plagioclase paragenesis observed on separated mounts and thin sections all represented various P/T conditions (Fig. 7b). Amphibole and biotite minerals were also identified, which support the presence of late crystallization conditions at superficial crustal levels at Lastarria (e.g., no amphibole present at depths >20 km according to Stechern et al., 2017). This indicates that magma evolution occurs at various depth ranges beneath Lastarria. The complex data related to the crystallizing magma reservoir beneath this volcano indicate that static magmas evolve both under deep and superficial conditions.

Overall, the data produced by this study support the frequent occurrence of mixing of variably differentiated materials in Lastarria magmas at different depth zones (up to 32 km) at least during the ascent of ignimbrite sequences between ~4.8 and 2.5 ky (Naranjo, 2010). Depth zones for mixing (e.g., Naranjo, 1992) with mafic endmembers were identified down to 18 km by Stechern et al. (2017) (Fig. 10b), and they are supported by our data obtained from the mineral chemistry analyses and our observed mingling bands of clear and dark tones from LRA3 and LRA4 pumices. The scenario of mafic magma injection and mixing of different endmember compositions is supported by our scoriae and pumice fragments of different ages (<4.8 ky), where inverse zoning is present in mafic minerals (Fig. 3b, d, f). This is evidenced in various single core–rim pairs of Mg# values of single phenocrysts (Appendixes II–V).

5.2. Primitive magma composition, influence from subducting slab and processes occurring during magma ascent in the crust

The findings from the bulk-rock analyses of our samples were compared at Lascar and Lastarria volcanoes to verify the magma affinity and characterize the extent of differentiation from primitive magmas (Tables 1 and 2). Lascar volcano magmas show an Andean–continental-island-arc affinity for HFSE and transition-metal ratio (Sc/Ni) markers, while La/Yb and Sc/Ni in Lastarria samples are typical of Andean magmatism and plot among the field of volcanic rocks from northern CVZ (Fig. 8a). The mafic origin of most Lascar products reflects a low magma differentiation, such as being less rich in K and corresponding to a homogeneous source, and so restricted to a typical volcanic arc signature (Fig. 8b). The tectonic environment signature is similar, but even though the data set is very small, the La/Yb and Sr/Y ratios clearly support that the crustal contribution to the genesis of magma is greater for Lastarria where elevation and crust thickness are expected to be greater (Chiaradia, 2015; Hildreth and Moorbath, 1988; Stern, 2004; Thorpe, 1982). This highlights the common association with Andean K-rich magmas (Stern, 2004) and reflects the regional variations of Quaternary volcanic systems north of the CVZ, although still within the calc-alkaline range (Fig. 8b).

To verify if the MORB signature of magma was modified, bulk-rock results were plotted in a discrimination diagram where lines divide subduction from nonsubduction settings and arrows point to MORB and within-plate granite endmembers (Fig. 8b). The purple star in the figure indicating primordial mantle is from Bowden et al. (1984), which approximately divides ocean arcs from active continental margins. The evolution of K_2O/Yb versus Ta/Yb shows that both volcanoes erupted products affected by fractional crystallization (Fig. 8b).

The concentrations of trace elements and REEs from bulk-rock analyses of both Lascar and Lastarria share familiar characteristics, such as both representing typical MORB and tholeiitic series. Since bimodal mantle and crustal magma origin are identified at Lastarria and are typical of Andean rocks, we suggest that various local factors can affect the bulk-rock chemistry and be superimposed over MORB signatures (Davidson and de Silva, 1992). The plate-rock enrichment in an intercontinental context probably reflects a certain mantle MORB signature modification at Lastarria via crustal contamination during episodes of magma stagnation (Fig. 8b). The composition variations are concordant with longer magmatic cycle pauses between ignimbrite sequences, to at least three extrusive events occurring since ~4.8 ky (Naranjo, 2010). This chemical variation is far from reflecting large-volume Andean ignimbrites emitted during long-term tectonic cycles covering millions of years (e.g., de Silva et al., 2006; Scott et al., 2018; Wörner et al., 2018), and so bulk-rock chemistry contamination at the scale of the

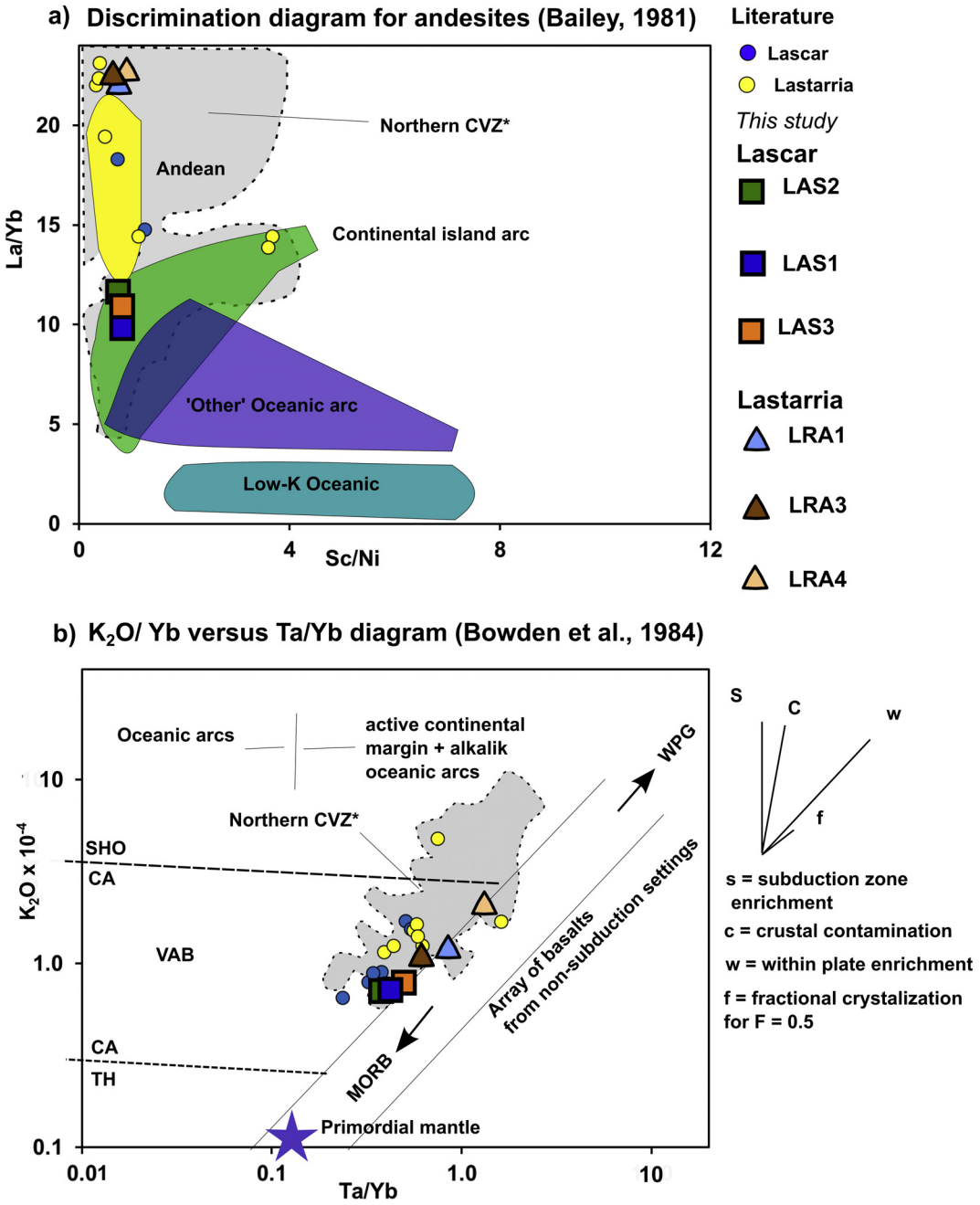

Fig. 8. Rock classification diagram. Results from Lascar and Lastarria bulk-rock chemistry analyses. (a) Tectonic discrimination of the andesites (Bailey, 1981). The tectonic discrimination diagrams of La/Yb versus Sc/Ni are from Bailey (1981), which provide evidence for each tectonic environment while highlighting the common association with Andean magmas. HFSE Sc versus transition-metal Ni marker for a mafic origin. b) Tectonomagmatic environment (Bowden et al., 1984). Diagram of K_2O/Yb versus Ta/Yb where the tectonomagmatic environment provides evidence from the discrimination diagrams of Bowden et al. (1984) reporting Yb (LREE). Lines divide subduction from nonsubduction settings and arrows point to MORB and within-plate granite (WPG) endmembers. The purple star indicating primordial mantle is from Bowden et al. (1984), which approximately divides ocean arcs from active continental margins; central Andes and volcanic arc basalts are also from that study. Shoshonitic (SHO), CA, and tholeiitic (TH) series are shown to also be consistent with mobile major-element diagrams in the other figures. Vectors on the right-hand side indicate different factors that may affect the bulk-rock distribution. Literature data are listed in Scheinost (2018). (For interpretation of the references to colour in this figure legend, the reader is referred to the web version of this article.)

vertical plumbing system may represent basement heterogeneities (Haschke et al., 2006; Wörner et al., 1994).

At Lascar this dual chemical characteristic is not present in the magmas that has intruded into the crust since ~9.2 ky, at least for the samples analyzed in the present study, since Fig. 8b shows a typical volcanic arc signature with a lower crustal influence (low K_2O/Yb and La/Yb ratios; Ibid. for Sr/Y). The chemistry of bulk rock represents a less-contaminated composition of one particular major magmatic cycle during the 1980s and 1990s and an older volcanic event from the Holocene. This extent of MORB modification from Lascar magma probably represents shorter residence times for the "crystal mush" systems modeled in Fig. 10a.

We finally consider some key incompatible trace elements ratios [Ba/La, U/Th, Sm/La, Ba/Th (not shown)] measured in bulk rocks from Lascar, Lastarria and other volcanoes from CVZ in order to evaluate the contribution of sediments, fluids and slab melts to the mantle wedge composition beneath this arc segment of CVZ (Fig. 11). In fact, previous studies already recognized that high Ba/La and U/Th values are

indicative of an important involvement in the magma genesis by subducting sediments (Patino et al., 2000; Sadofsky et al., 2008 and references therein), as well as high Ba/Th values are inherited by aqueous fluid from the subducting slab (e.g., Turner and Hawkesworth, 1998 and references therein). This was observed e.g. in CAVA for Nicaraguan volcanoes (Sadofsky et al., 2008 and references therein). Our samples, however, have low Ba/La, U/Th, and Ba/Th (mean values 17.8, 0.3, and 64.6 for Lascar and 13.6, 0.3, and 24 for Lastarria, respectively), and cluster near depleted MORB-source mantle (DMM) (Fig. 11a). This likely indicates that the contribution of subducting sediments and fluids to magma genesis is very low in the wedge below Lascar and Lastarria, and most of CVZ volcanoes, in accordance with evidences from previous studies (Bourdon et al., 2000; Rosner et al., 2003).

When Ba/La is compared to La/Sm, it is possible to evaluate either the contribution to magma genesis by fluids and sediments or whether the slab components that are added to the mantle wedge have melt-like properties (Sadofsky et al., 2008). We already discussed the Ba/La values for rocks from Lascar, Lastarria, and most of CVZ volcanoes, excluding an important contribution of sediments and fluids to the wedge. Instead, in Fig. 11b we notice that the La/Sm values are medium-high for the studied volcanoes and other from CVZ, suggesting either the involvement of an enriched mantle or a melt-like component derived from the magmatic portion of the downgoing slab, as hypothesized in CAVA for Costa Rican magmas (Sadofsky et al., 2008).

Therefore, from trace element geochemistry, we argue that significant differences in the mantle wedge composition beneath Lascar and Lastarria, and probably also beneath the other volcanoes of CVZ can be ruled out.

5.3. Geochemistry of FIs and fumarole gases

5.3.1. Atmospheric contamination

The $^{4}He/^{20}Ne$ and $^{40}Ar/^{36}Ar$ ratios of fumarole gases and FIs from Lastarria and Lascar highlight a variable but high extent of air contamination. In general, this contamination is comparable among the studied samples, although fumarole gases display a slightly minor addition of air relative to FIs, as indicated especially by their higher $^{4}He/^{20}Ne$ ratios (Fig. 6) (Tables 3 and 4). The $^{4}He/^{20}Ne$ ratios from Lastarria and Lascar are comparable or within the range of those obtained in fumarole gases from previous studies ($^{4}He/^{20}Ne$ = 34–142, Tassi et al., 2009; $^{4}He/^{20}Ne$ = 38–648, Aguilera et al., 2012; $^{4}He/^{20}Ne$ = 160–199, Lopez et al., 2018). These different ranges of values could be likely due to the distinct sampling conditions and timing as well as to a possible different state of activity (i.e., flux of gas) of the volcanoes. However, the $^{4}He/^{20}Ne$ and $^{40}Ar/^{36}Ar$ ratios of fumarole gases and FIs are well below the reported MORB-like values ($^{4}He/^{20}Ne > 1000$ and $^{40}Ar/^{36}Ar \leq 44{,}000$; e.g., Burnard et al., 1997; Ozima and Podosek, 2002).

A possible explanation to the air contamination of fumarole gases from Lastarria and Lascar involves a shallow fracturing of the soil close to the emission areas and/or the recycling of meteoric water in the hydrothermal system of the volcanoes. However, we point out that fumarole gases from Lastarria were sampled from a high-temperature emission located within a fumarole field characterized by the huge degassing of magmatic-like gases that strongly contribute to the total SO_2 flux emitted from this volcano (Lopez et al., 2018 and references therein).

Instead, the atmospheric contamination found within FIs could be related to the entrapment of air in mineral micro cracks formed in post-eruptive conditions, as already proposed by Nuccio et al. (2008). Differently, the adsorption of atmospheric gases onto the surfaces of mineral grains (Protin et al., 2016) can be excluded because we handpicked crystals greater than 250 μm in size.

Nevertheless, if we consider the $^{4}He/^{20}Ne$ and $^{40}Ar/^{36}Ar$ ratios of fumarole gases and FIs from Lastarria and Lascar and those measured in other arc volcanoes on Earth (Battaglia et al., 2018; Di Piazza et al., 2015; Hilton et al., 2002; Martelli et al., 2014; Oppenheimer et al., 2014; Rizzo et al., 2015, 2019; Robidoux et al., 2017; Sano and Fischer, 2013; Shaw et al., 2003, 2006; Taran, 2009), we still find comparable ranges of values that remain well below the expected MORB ratios ($^{4}He/^{20}Ne > 1000$ and $^{40}Ar/^{36}Ar \leq 44{,}000$; e.g., Burnard et al., 1997; Ozima and Podosek, 2002). We highlight that in subduction-related settings the atmospheric component is also recycled into the mantle by subducting slabs (e.g., Yamamoto et al., 2004). In support of this hypothesis, we highlight that mantle xenoliths from Avacha volcano (Kamchatka), which offer a very rare opportunity on Earth of a direct access to a mantle wedge below arc volcanoes, show $^{4}He/^{20}Ne < 850$ and $^{40}Ar/^{36}Ar$ values <400 (Hopp and Ionov, 2011; Kobayashi et al., 2017), as observed in fumaroles from the same volcano (Taran, 2009). Therefore, we argue that the presence of an atmospheric component in the magmatic and/or mantle source below Lastarria and Lascar cannot be ruled out, while it likely is an intrinsic feature of this type of geodynamic settings.

5.3.2. Definition of the $^{3}He/^{4}He$ signature of Lascar and Lastarria magmatic fluids

We evaluated the geochemical features of magmatic/mantle sources beneath Lascar and Lastarria, by focusing on $^{3}He/^{4}He$ corrected for air contamination (Rc/Ra). We also considered $^{4}He/^{40}Ar^{*}$, when available, because this tracer is proxy of magmatic degassing in phenocrysts and fumaroles (e.g., Boudoire et al., 2018 and references therein) and is useful to recognize diffusive loss of helium from crystals that may lower the $^{3}He/^{4}He$ values of FIs (e.g., Burnard, 2004). This is because He is around 10 times more soluble than Ar in silicate melts, although this difference can vary due to the chemistry and pressure of magmas, leading eventually to $^{4}He/^{40}Ar^{*}$ increasing especially during the late stages of degassing (e.g., Boudoire et al., 2018; Iacono-Marziano et al., 2010). Concerning FIs, helium is more prone to diffuse from crystal than the other noble gases (e.g., $D^{4}He/D^{40}Ar = 3.16$ in solid mantle; Burnard, 2004). It should be noted that the $^{4}He/^{40}Ar^{*}$ ratio in the upper mantle has a production ratio of 1–5 (Marty, 2012), thus ratios in FIs of phenocrysts much below this range could be an indirect proxy of the occurrence of diffusive fractionation.

As reported in Sections 4.4.1 and 4.4.2, the Cpx from LAS1 and the cogenetic olivine and Cpx from LAS3 show Rc/Ra values between 6.9 and 7.3 Ra, while Cpx xenocrysts of LAS1 display lower values of 5.2–5.4 Ra (Figs. 5 and 6). The $^{3}He/^{4}He$ ratios measured in LAS1 and LAS3 phenocrysts are comparable to the range of values measured in fumarole gases of Lascar by Tassi et al. (2009) (6.5–7.3 Ra). Considering that geobarometric modeling (Section 5.1.1) estimates a depth of crystallization between ~11 and ~20 km (305 and 546 MPa) for the magma that produced our most recent sample LAS1 (Fig. 10a), we argue that fumarole gases could be fed by a magma ponding at that level of the Lascar plumbing system. This implies that the $^{3}He/^{4}He$ signature of this magma does not experience any shallow contamination (e.g., in the hydrothermal system) by crustal-derived ^{4}He. Another implication arising from the high $^{3}He/^{4}He$ values in fumarole gases is that the state of activity of this volcano can be considered high in accordance with the recent occurrence of phreatic explosions coupled to seismicity (Gaete et al., 2019; Gaete Rojas et al., 2020) and the presence of other magmatic indicators (i.e., SO_2; Tamburello et al., 2014, Layana et al., 2020) in fumarole gases.

Instead, the lower $^{3}He/^{4}He$ values measured in Cpx xenocrysts from LAS1 than LAS1 and LAS3 phenocrysts (Fig. 5) could reflect i) diffusive loss of helium from crystals, ii) crustal assimilation, or iii) magma aging. We exclude a diffusive loss of helium from xenocrysts of LAS1, because they show a concentration of ^{4}He comparable or even higher than Cpx from LAS1 and of olivine and Cpx from LAS3 (Fig. 5) and $^{4}He/^{40}Ar^{*}$ of 5.0–6.1 that are higher than other phenocrysts from Lascar (Table 4). We do not have constraints to discuss the hypothesis of crustal assimilation. However, based on the geochemistry of rocks that suggest a moderate crustal contamination (Mamani et al., 2008, 2010; this work) this process seems unlikely. For modeling magma aging, we considered the equation of radiogenic ^{4}He production from a-decay of the

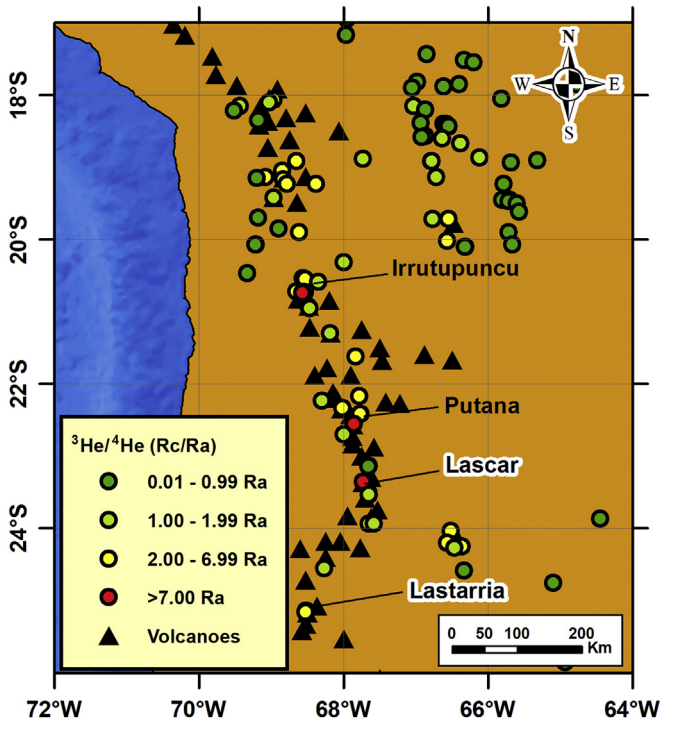

Fig. 9. Spatial distribution of Rc/Ra in geothermal and volcanic gases from northern Chile. The locations of volcanoes are shown with black triangles. Lascar and Lastarria are indicated by blue triangles with black centered dots. The Rc/Ra values of geothermal and volcanic gases are shown as circle differently colored in function of the range of values, as explained in the legend. Data sources are Hilton et al. (1993), Hoke et al. (1994), Tassi et al. (2009, 2011), Aguilera et al. (2012) and Lopez et al. (2018). (For interpretation of the references to colour in this figure legend, the reader is referred to the web version of this article.)

^{235,238}U and ^{232}Th decay proposed by Ballentine and Burnard (2002) and assumed the concentrations of U and Th measured in the sample LAS1. We calculated that about 1500 years of magma aging would produce sufficient moles of radiogenic ^{4}He to lower the ^{3}He/^{4}He values measured in Cpx phenocrysts from LAS1 (7.1 Ra) to the values measured in Cpx xenocrysts from LAS1 (5.3–5.5. Ra). To be effective, this process should occur in a magma that differentiated and degassed in the Lascar plumbing system over a long time. This hypothesis is reasonable since LAS1 xenocrysts represent augite (cumulates) that may have experienced a lower cooling rate and a longer residence time for the dome fragment formed during 1986–1993 (Section 5.1.1). This idea is qualitatively supported by the ^{4}He/^{40}Ar* ratio, which is higher in Cpx xenocrysts from dome fragment LAS1 (^{4}He/^{40}Ar* = 5.0–6.1; Table 4) than in samples displaying the highest ^{3}He/^{4}He ratios (LAS1 and LAS3) (^{4}He/^{40}Ar* = 1.2–2.1), confirming that Cpx xenocrysts experienced a relative higher extent of magmatic degassing. Therefore, to explain the low ^{3}He/^{4}He ratios of Cpx xenocrysts from LAS1, we consider more likely the hypothesis of magma aging.

In the case of Lastarria volcano, FIs showed ^{3}He/^{4}He ratios between 5.3 and 8.0 Ra (Figs. 5, 6 and 9). The highest value (8.0 Ra) was uniquely measured in the olivine of LRA3, while lower values (5.3–6.6 Ra) were measured in Cpx of LRA3 and LRA4, which represent magmas from Ignimbrites 1 and younger magmatic recharges <4.8 Ky (Table 4). We argue that it is quite common that FIs of olivine reflect a more-primitive signature of ^{3}He/^{4}He than cogenetic Cpx augite-type that often are not in equilibrium (e.g., Shaw et al., 2006; Nuccio et al., 2008 and references therein; Di Piazza et al., 2015; Rizzo et al., 2015; Robidoux et al., 2017). These latter minerals seem to reflect a later (shallower) stage of magma degassing (Fig. 10b), being thus more prone to the contamination by crustal-derived ^{4}He in the shallower

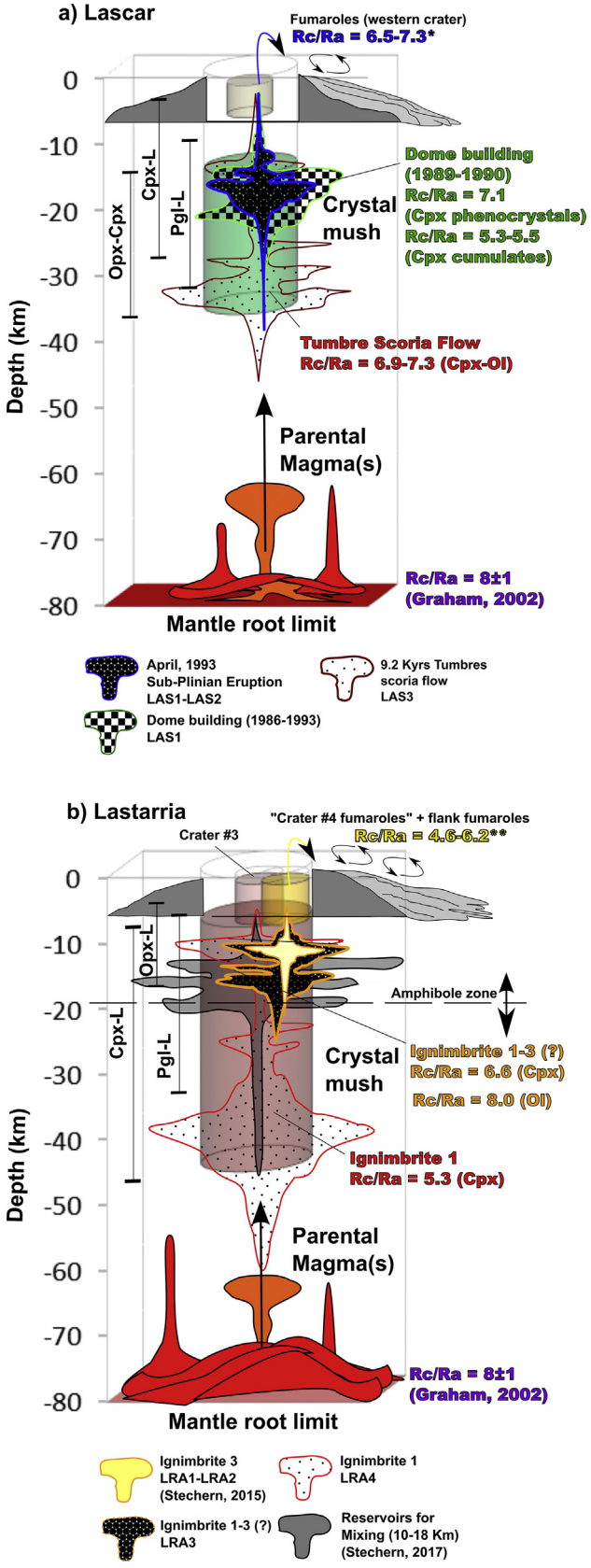

Fig. 10. Derived equivalent lithostatic pressure model for ascending magmas. ^{3}He/^{4}He ratios corrected for atmospheric contamination (Rc/Ra) are associated with magma recharge events at (a) Lascar and (b) Lastarria. The Rc/Ra values from fumaroles are taken considering data validation in Section 5.3.2 and 5.3.3. Vertical scale is conserved for equivalent depth (km), but lateral extensions of magma reservoirs are interpreted.

parts of the volcano plumbing system. This effect can be even more frequent when the continental crustal thickness is high, as below this segment of South American Andes (Thorpe, 1982).

The fumarole gases analyzed in this work have a mean $^3He/^4He$ ratio of ~5.3 Ra, which is within the range of previous measurements in fumarole gases (4.6–6.2 Ra) by Aguilera et al. (2012) and Lopez et al. (2018) (Figs. 5 and 10b). Therefore, $^3He/^4He$ ratios of fumarole gases match those from FIs in Cpx of LRA3 and LRA4, suggesting the occurrence of crustal contamination. The evidence from petrography and mineral chemistry (Section 5.2) indicates that fractional crystallization processes plus crustal assimilation during multistep ponding of magmas could explain the observed variability at Lastarria in $^3He/^4He$ ratios between olivine and Cpx.

5.3.3. Inferences on the mantle sources beneath Lascar and Lastarria volcanoes

In order to draw conclusions about the local mantle source, we consider the highest $^3He/^4He$ values measured in FIs from Lascar and Lastarria. The $^3He/^4He$ value of 7.3 Ra measured in FIs from Lascar falls within the lower end of the MORB range (8 ± 1 Ra; Graham, 2002), while that of 8.0 Ra in FIs from Lastarria is around the middle of the MORB range (Figs. 5 and 6). Compared to South American volcanism, the $^3He/^4He$ ratios measured in FIs from Lascar and Lastarria are the highest ever measured in volcanic gases from the CVZ (up to 7.1–7.3 Ra at Irruputuncu and Putana volcanoes; Tassi et al., 2011) (Fig. 9), while they are comparable to the highest values measured in geothermal gases from Cordon Caulle (up to 7.3 Ra; Sepúlveda et al., 2007), as well as in volcanic gases from the Planchón-Peteroa (7.1 Ra; Tassi et al., 2016) and the Caviahue-Copahue Volcanic Complex (7.9 Ra; Agusto et al., 2013; Roulleau et al., 2016, 2018; Tassi et al., 2017), all located in the Southern Volcanic Zone (SVZ) of Chile. In comparison, the only available data of FIs for volcanoes from CVZ (including Lascar) and SVZ display Rc/Ra values up to 6.0 and 6.9 Ra, respectively (Hilton et al., 1993). However, it must be considered that Hilton et al. (1993) studied FIs through multi-step crushing technique, which is less conservative than the single-step one (this study), favoring the mixing of FIs with cosmogenic ^3He and radiogenic ^4He sited in the crystal matrix (e.g., Hilton et al., 2002; Kurz, 1986; Rizzo et al., 2015).

Another consideration that arises from this and past studies of $^3He/^4He$ in South American volcanism is that only fumarole gases from very active volcanoes (i.e., degassing SO_2 into the atmosphere) and FIs in olivine and pyroxene analyzed via single-step crushing yield values that can be used for extrapolations to magmatic/mantle features. In the case of FIs, this is even more valid if the composition of FIs correlates with the lowest level of magma differentiation (e.g., low bulk rock SiO_2 wt% and elevated Mg#; Caviahue-Copahue; Roulleau et al., 2018). Instead, $^3He/^4He$ ratios measured in geothermal fluids and fumaroles from volcanoes exhibiting little activity (with no active SO_2-rich plume) or quiescent volcanoes (e.g., Benavente et al., 2016; Hilton et al., 1993; Ray et al., 2009; Tardani et al., 2016; Tassi et al., 2011, 2016 and references therein) are very often below the MORB range, indicating variable extents of crustal contamination (Fig. 9). These extents of contamination seem also to be related to the crust thickness and how far the gas emissions are from the arc front and the main eruptive vents, as observed in other volcanic context on Earth (Hilton et al., 2002; Sano and Fischer, 2013). For example, the fumaroles ($n = 3$) sampled farthest from the active volcanic front fall below the $^3He/^4He$ range of 0.82–6.02 Ra reported for CVZ by Hilton et al. (1993). Contrary to SVZ of Chile, where Rc/Ra values of fumarole gases progressively increases from north to south with a decreasing contribution from continental crustal ^4He (Benavente et al., 2016), there is no clear north–south variation in CVZ (Veloso et al. (2019) (Fig. 9). Instead, the $^3He/^4He$ ratios decrease as the thickness of the rigid continental crust increases toward the east of the Andean cordillera (Gardeweg et al., 2011). The latter evidence supports the idea that crustal thickness plays an important role in lowering the $^3He/^4He$ values and could explain most of the Rc/Ra

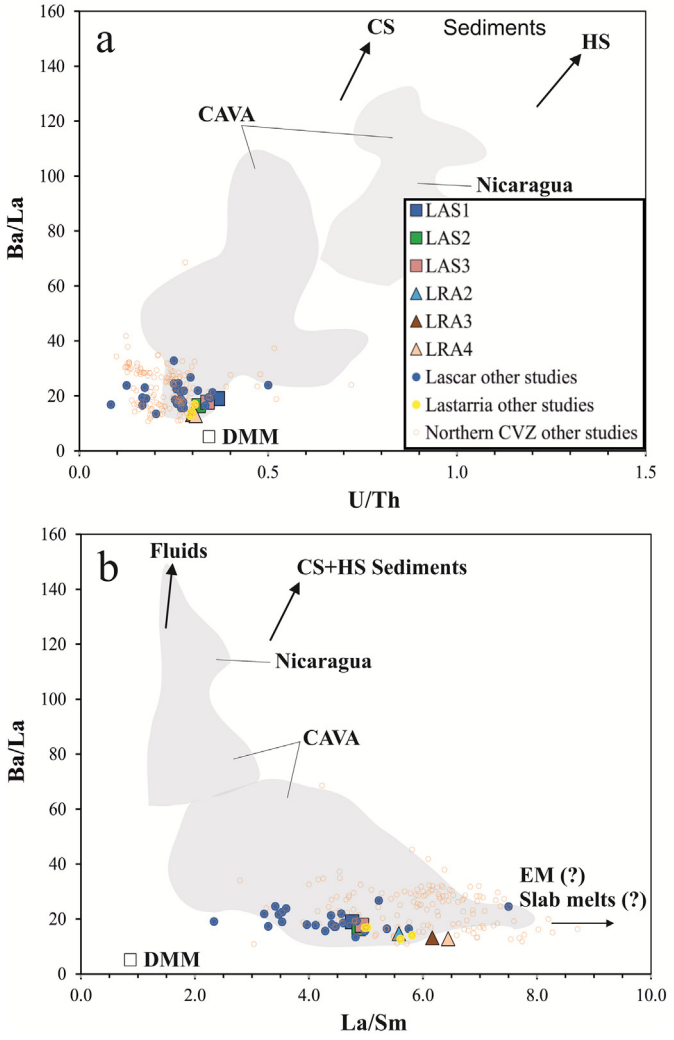

Fig. 11. Incompatible trace elements variations in bulk rocks. A) U/Th vs Ba/La and B) La/Sm vs Ba/La plots. CS and HS indicate compositions of carbonate and hemipelagic sediments, respectively, and are taken from a detailed study carried out in rocks from CAVA (Patino et al., 2000; Sadofsky et al., 2008 and references therein). Literature data of CVZ are from Deruelle (1982), Baker et al. (1987), Wörner et al. (1988), Feeley (1993), Feeley and Davidson (1994), Wittenbrink (1997), Kohlbach and Lohnert (1999), Matthews et al. (1999), Trumbull et al. (1999), Figueroa (2006), Grunder et al. (2008), Mattioli et al. (2006), Hora et al. (2007), Lamb and Hoke (2007), Kiebala (2008), Ortega (2008), Mamani et al. (2008, 2010), Hoffmann (2011), Banaszak (2014), Godoy (2014), Godoy et al. (2014), Menard et al. (2014), Cascante (2015), and Ureta (2015). DMM is the composition of depleted MORB mantle source (Salters and Stracke, 2004). EM stands for enriched mantle (Sadofsky et al., 2008 and references therein).

values at the lower end or even lower than MORB range measured in CVZ and SVZ. This would imply that a contamination of the mantle wedge by subducting sediments and/or slab fluids rich in U and Th is an unlikely explanation for this arc segment. However, we do not exclude that other regional factors (i.e., structural geology and evolution of the geodynamic; Tardani et al., 2016; Roulleau et al., 2018) could play a complementary role in lowering the $^3He/^4He$ values, although we consider it unlikely at least for NVZ.

From a general point of view, the $^3He/^4He$ values measured in FIs from Lascar and Lastarria fall within the range of ratios reported for most of the volcanic arc segments worldwide (e.g., Colombian Andes, Lesser Antilles, the Sunda arc system in Sumatra and Bali, Central American Volcanic Arc, Kamchatka and Kuriles Island; Sano et al., 1997; Hilton et al., 2002; Shaw et al., 2006; Taran, 2009; Sano and Fischer, 2013; Völker et al., 2013; Jacques et al., 2014; Di Piazza et al., 2015; Robidoux et al., 2017; Battaglia et al., 2018). In Fig. 5, for

comparison with Lascar and Lastarria, we report the $^3He/^4He$ measurements carried out in FIs of volcanic rocks from CAVA. We choose this arc segment because it was extensively studied for noble gas in fumarole gases and FIs (Battaglia et al., 2018; Di Piazza et al., 2015; Robidoux et al., 2017; Shaw et al., 2003, 2006 and references therein), and displayed along-arc variations of many petrological and geochemical tracers induced by the variable subduction conditions and subducting sediments, fluids compositions or slab melts (e.g., Aiuppa et al., 2014; Patino et al., 2000; Sadofsky et al., 2008 and references therein). In detail, the $^3He/^4He$ measurements of FIs from CAVA show values around 7.0–7.5 Ra in Nicaragua (Robidoux et al., 2017; Shaw et al., 2006), ~8 Ra in Costa Rica (Di Piazza et al., 2015; Shaw et al., 2006), and up to 9.0 Ra in Guatemala (Pacaya volcano; Battaglia et al., 2018), whose values are among the highest ever measured in arc volcanoes on Earth (Hilton et al., 2002; Sano and Fischer, 2013) (Fig. 5). The lowest $^3He/^4He$ values measured in FIs from Nicaraguan volcanoes could reflect contamination of the wedge by U- and Th-rich slab sediments and fluids (Robidoux et al., 2017), as inferred from rocks geochemistry (Patino et al., 2000; Sadofsky et al., 2008). This leads us to initially supposing that $^3He/^4He$ values of 7.3 Ra measured in FIs from Lascar could reflect a mantle wedge contamination similar to that hypothesized for Nicaraguan volcanoes. However, the geochemistry of minerals and rocks (Section 5.2) highlights that magma differentiation and a moderate crustal contamination (Mamani et al., 2008, 2010) likely occur beneath Lascar. Additionally, the influence to the wedge composition beneath the studied volcanoes by subducting sediments and slab fluids seems minor if compared to e.g. CAVA segment (Fig. 11) (e.g., Patino et al., 2000; Sadofsky et al., 2008 and references therein).

Considering the above evidence and the large thickness of continental crust (about 71 km; Thorpe, 1982) beneath this portion of South American Andes, it seems more likely that the difference in $^3He/^4He$ values between the studied volcanoes is attributable to local influence by crustal contamination.

6. Conclusions

In this study, we investigated the chemistry of mineral and rocks erupted from Lascar and Lastarria volcanoes, located in CVZ of South American Andes, in combination with noble gas measurements of fluid inclusions (FIs) in olivines and clinopyroxenes (Cpx) separated from the same suite of samples. The main outcomes are below summarized.

According to the petrological data from bulk rocks and mineral separates (olivine, ortho-Cpx, and plagioclase), at Lascar ascending magmas are ponding in distinct zones within the crust, whose depths were constrained with P/T models as crystallizing Opx equilibrium ranges (305–546 MPa, corresponding to lithostatic equivalent depths [LEDs] of 11–20 km). The Cpx and Plagioclases track the chemical variations of mafic magmas from Tumbres scoria flow and 1980–1990s, showing distinct P-T decompression paths and reaching a shallow ponding zone (<305 MPa; [LEDs] of 11 km). This is a key-level of the plumbing system at which we presume changing cooling/crystallizing rates guide their pre-eruptive conditions until ascending into the last 5 km of vertical rigid plumbing system (Gaete Rojas et al., 2020).

In contrast, Lastarria is fed by a more complex plumbing system characterized by multiple magmatic recharges occurring under the deepest crustal conditions (~500–990 MPa, corresponding to LEDs of ~20–40 km; ibid. Stechern et al., 2017). Overall, our study highlights that in the deepest magma storage (between ~10 and 18 km; Stechern et al., 2017) mixing between magmas are taking place, coinciding to limit P/T conditions of amphibole (Ridolfi et al., 2010; Ridolfi and Renzulli, 2012; Stechern et al., 2017). In the shallow portion of the plumbing system, Cpx and Opx can equilibrate until a minimum depth of 6.5–8 km, while at depths between 1 and 5–6 km pond the most-differentiated magmas and residual fluids responsible of deformation measured at the surface (Díaz et al., 2015; Remy et al., 2014; Spica et al., 2015).

The geochemistry of bulk rocks indicates a lower magma differentiation at Lascar than at Lastarria, which shows a greater crustal contribution to the genesis of magma. This agrees with the reconstruction of the plumbing system based on mineral chemistry modeling, which results in a more complex multi-ponding system beneath Lastarria.

The evaluation of some key incompatible trace elements ratios [Ba/La, U/Th, Sm/La, Ba/Th (not shown)] suggests a minor contribution of sediments and fluids, and a moderate involvement of slab melts to the mantle wedge composition beneath this arc segment of CVZ. Thus, we argue that the mantle wedge composition beneath Lascar and Lastarria, and probably also beneath the other volcanoes of CVZ, can be considered homogeneous.

The noble gas composition of FIs hosted in mafic minerals separated from Lascar and Lastarria rocks and of fumaroles (from Lastarria only), integrated by previous measurements in fumarole gases from both volcanoes, revealed some degree of air contamination. This contamination is likely characteristics of the local magmatic/mantle sources as in many other worldwide subduction-related volcanoes, although post-eruptive addition in crystals or extraction of atmospheric fluids from the local hydrothermal systems in fumarole gases cannot be ruled out.

The $^3He/^4He$ values showed a certain variability in both magmatic systems (i.e., 5.3–7.3 Ra for Lascar and 5.3–8.0 for Lastarria), with the highest values that are within the range of MORB and of many other volcanic arc segments on Earth, and can be thus considered representative of the $^3He/^4He$ signatures of local magmatic fluids. At Lascar, the highest $^3He/^4He$ values (6.9–7.3 Ra) are comparable to those of fumarole gases, indicating that the crustal contamination or magma aging are not occurring in the last 11 km. Instead, the lowest $^3He/^4He$ values measured in some Cpx xenoxrysts of probable cumulitic origin suggest that they crystallized from a differentiated and degassed melt ponding at shallow levels of the plumbing system and that they suffered about 1500 years of aging. At Lastarria, in olivine crystals we measured the highest $^3He/^4He$ (8.0 Ra) ever measured in this volcano. The other Cpx samples showed lower ratios (5.3–6.6 Ra) within the range of values measured in fumarole gases (4.6–6.2 Ra). This implies that Cpx crystallized at a shallower depth than olivine from a more degassed and differentiated melt that was contaminated by crustal-derived ^4He, supporting the presence of multi-ponding zones of magma within the plumbing system highlighted by mineral chemistry modeling and rock geochemistry. Magma feeding fumarole gases would likely have geochemical features similar to that from which Cpx crystallized.

We conclude that the different $^3He/^4He$ signatures inferred for the magmatic sources feeding Lascar and Lastarria (7.3 and 8.0 Ra, respectively), despite the similarities in their explosive volcanic behaviors and geological backgrounds, likely results from a local crustal contamination beneath Lascar rather than from a mantle heterogeneity of $^3He/^4He$ ratio beneath CVZ.

Declaration of Competing Interests

The authors declare that they have no known competing financial interests or personal relationships that could have appeared to influence the work reported in this paper.

Acknowledgments

We thank the Director of INGV-Palermo and Fausto Grassa for providing access to the analytical facilities. We also thank the DiSTeM laboratory at the University of Palermo for supporting this work with internship opportunities. Special thanks are due to Mariano Tantillo and Mariagrazia Misseri for helping in sample preparation and noble-gas analyses in the INGV-Palermo isotopic laboratory, as well as to Piergiorgio Scarlato for allowing access to the HPHT laboratory of INGV in Rome for electron microprobe analysis. We also would like to

mention the field participation of Universidad Católica del Norte in Antofagasta and the organizer of the 2014 IAVCEI CCVG 12th Volcanic Gas Workshop in Chile, who made access possible for field rock sampling; that workshop also provided a student travel scholarship of US$ 1,000. This work was partially supported by the Deep Carbon Observatory. Philippe Robidoux is funded by Fondo Nacional de Desarrollo Científico y Tecnológico, ANID/Fondecyt de Iniciación/11190846. Philippe Robidoux acknowledges FONDAP Project 15090013 granted to the Andean Geothermal Centre of Excellence (CEGA). Andrea Luca Rizzo and Alessandro Aiuppa acknowledge funding from the Ministry of Education, Universities and Research (MIUR) under grant PRIN2017-2017LMNLAW. Felipe Aguilera is funded by Centro de Investigación para la Gestión Integrada del Riesgo de Desastres (CIGIDEN), ANID/FONDAP/15110017. English was revised by English Science Editing (ESE, Paul Kolston). We are grateful to the Editors of Lithos and two anonymous Reviewers for the suggestions that strongly improved the manuscript.

Appendix A. Supplementary data

Supplementary data to this article can be found online at https://doi.org/10.1016/j.lithos.2020.105615.

References

Aguilera, F., 2008. Origin and evolution of fluid in volcanoes, geothermal fields and thermal discharges of Central Volcanic Zone in northern Chile (17°43' S–25°10' S). Doctoral dissertation, Ph. D. thesis. Univ. Catol. Norte, Chile (in Spanish).

Aguilera, F., Viramonte, J., Medina, E., Guzmán, K., Becchio, R., Delgado, H., Arnosio, M., 2006, August. Eruptive activity from Láscar volcano (2003–2005). 11th Chilean Geological Congress, Antofagasta, Chile, pp. 397–400.

Aguilera, F., Tassi, F., Darrah, T., Moune, S., Vaselli, O., 2012. Geochemical model of a magmatic–hydrothermal system at the Lastarria volcano, northern Chile. Bull. Volcanol. 74 (1), 119–134.

Agusto, M., Tassi, F., Caselli, A.T., Vaselli, O., Rouwet, D., Capaccioni, B., Caliro, S., Chiodini, G., Darrah, T., 2013. Gas geochemistry of the magmatic-hydrothermal fluid reservoir in the Copahue–Caviahue Volcanic Complex (Argentina). J. Volcanol. Geotherm. Res. 257, 44–56.

Aiuppa, A., Robidoux, P., Tamburello, G., Conde, V., Galle, B., Avard, G., Bagnato, E., De Moor, J.M., Martínez, M., Muñoz, A., 2014. Gas measurements from the Costa Rica–Nicaragua volcanic segment suggest possible along-arc variations in volcanic gas chemistry. Earth Planet. Sci. Lett. 407, 134–147.

Andres, R.J., Kasgnoc, A.D., 1998. A time-averaged inventory of subaerial volcanic sulfur emissions. J. Geophys. Res. Atmos. 103 (D19), 25251–25261.

Bailey, J.C., 1981. Geochemical criteria for a refined tectonic discrimination of orogenic andesites. Chem. Geol. 32 (1–4), 139–154.

Baker, P.E., González-Ferrán, O., Rex, D.C., 1987. Geology and geochemistry of the Ojos del Salado volcanic region, Chile. J. Geol. Soc. London 144 (1), 85–96.

Ballentine, C.J., Burnard, P.G., 2002. Production, release and transport of noble gases in the continental crust. Rev. Mineral. Geochem. 47 (1), 481–538.

Banaszak, M., 2014. Differentiation Regimes in the Central Andean Magma Systems: Case Studies of Taapaca and Parinacota Volcanoes, Northern Chile. Doctoral dissertation. Niedersächsische Staats-und Universitätsbibliothek Göttingen.

Batista Cruz, R.Y., Rizzo, A.L., Grassa, F., Bernard Romero, R., González Fernández, A., Kretzschmar, T.G., Gómez-Arias, E., 2019. Mantle degassing through continental crust triggered by active faults: The case of the Baja California Peninsula, Mexico. Geochem. Geophys. Geosyst. 20 (4), 1912–1936.

Battaglia, A., Bitetto, M., Aiuppa, A., Rizzo, A.L., Chigna, G., Watson, I.M., D'Aleo, R., Juárez Cacao, F.J., de Moor, M.J., 2018. The Magmatic gas Signature of Pacaya Volcano, with implications for the volcanic CO2 flux from Guatemala. Geochem. Geophys. Geosyst. 19 (3), 667–692.

Benavente, O., Tassi, F., Reich, M., Aguilera, F., Capecchiacci, F., Gutiérrez, F., Vaselli, O., Rizzo, A., 2016. Chemical and isotopic features of cold and thermal fluids discharged in the Southern Volcanic Zone between 32.5° S and 36° S: Insights into the physical and chemical processes controlling fluid geochemistry in geothermal systems of Central Chile. Chem. Geol. 420, 97–113.

Boudoire, G., Rizzo, A.L., Di Muro, A., Grassa, F., Liuzzo, M., 2018. Extensive CO2 degassing in the upper mantle beneath oceanic basaltic volcanoes: First insights from Piton de la Fournaise volcano (La Réunion Island). Geochim. Cosmochim. Acta 235, 376–401.

Bourdon, B., Wörner, G., Zindler, A., 2000. U-series evidence for crustal involvement and magma residence times in the petrogenesis of Parinacota volcano, Chile. Contrib. Mineral. Petrol. 139 (4), 458–469.

Bowden, P., Batchelor, R.A., Chappell, B.W., Didier, J., Lameyre, J., 1984. Petrological, geochemical and source criteria for the classification of granitic rocks: A discussion. Phys. Earth Planet. In. 35 (1–3), 1–11.

Bredemeyer, S., Ulmer, F.G., Hansteen, T.H., Walter, T.R., 2018. Radar path delay effects in volcanic gas plumes: The case of Láscar Volcano, Northern Chile. Remote Sens. (Basel) 10 (10), 1514.

Budach, I., Brasse, H., Díaz, D., 2013. Crustal-scale electrical conductivity anomaly beneath inflating Lazufre volcanic complex, Central Andes. J. South Am. Earth Sci. 42, 144–149.

Burnard, P., 2004. Diffusive fractionation of noble gases and helium isotopes during mantle melting. Earth Planet. Sci. Lett. 220 (3–4), 287–295.

Burnard, P., Graham, D., Turner, G., 1997. Vesicle-specific noble gas analyses of" popping rock": Implications for primordial noble gases in Earth. Science 276 (5312), 568–571.

Calder, E.S., Sparks, R.S.J., Gardeweg, M.C., 2000. Erosion, transport and segregation of pumice and lithic clasts in pyroclastic flows inferred from ignimbrite at Lascar Volcano, Chile. J. Volcanol. Geotherm. Res. 104 (1–4), 201–235.

Caracausi, A., Ditta, M., Italiano, F., Longo, M., Nuccio, P.M., Paonita, A., Rizzo, A., 2005. Changes in fluid geochemistry and physico-chemical conditions of geothermal systems caused by magmatic input: The recent abrupt outgassing off the island of Panarea (Aeolian Islands, Italy). Geochim. Cosmochim. Acta 69 (12), 3045–3059.

Cascante, M., 2015. Evolucion geologica y magmatica del volcan Isluga, 19°S. Region de Tarapaca, Chile.

Cashman, K.V., Edmonds, M., 2019. Mafic glass compositions: a record of magma storage conditions, mixing and ascent. Phil. Trans. R. Soc. A 377 (2139), 20180004.

Chiaradia, M., 2015. Crustal thickness control on Sr/Y signatures of recent arc magmas: An Earth scale perspective. Sci. Rep. 5, 8115.

Chiaradia, M., Pujol-Solà, N., Farré-de-Pablo, J., Aiuppa, A., Paonita, A., Rizzo, A.L., Brusca, L., 2018. Geochemistry and isotope composition (Sr, Pb, δ66Zn) of Vulcano fumaroles (Aeolian Islands, Italy). Chem. Geol. 493, 153–171.

Danyushevsky, L.V., Leslie, R.A., Crawford, A.J., Durance, P., 2004. Melt inclusions in primitive olivine phenocrysts: The role of localized reaction processes in the origin of anomalous compositions. J. Petrol. 45 (12), 2531–2553.

Davidson, J.P., de Silva, S.L., 1992. Volcanic rocks from the Bolivian Altiplano: Insights into crustal structure, contamination, and magma genesis in the central Andes. Geology 20 (12), 1127–1130.

De Silva, S.L., Francis, P.W., 1991. Volcanoes of the Central Andes. Springer-Verlag, Berlin.

De Silva, S., Zandt, G., Trumbull, R., Viramonte, J.G., Salas, G., Jiménez, N., 2006. Large ignimbrite eruptions and volcano-tectonic depressions in the Central Andes: A thermomechanical perspective. Geol. Soc. Lond. Spec. Publ. 269 (1), 47–63.

DeMets, C., Gordon, R.G., Argus, D.F., Stein, S., 1994. Effect of recent revisions to the geomagnetic reversal time scale on estimates of current plate motions. Geophys. Res. Lett. 21 (20), 2191–2194.

DeMets, C., Gordon, R.G., Argus, D.F., 2010. Geologically current plate motions. Geophys. J. Int. 181 (1), 1–80.

Deruelle, B., 1982. Petrology of the Plio-Quaternary volcanism of the south-central and meridional Andes. J. Volcanol. Geotherm. Res. 14 (1–2), 77–124.

Di Piazza, A., Rizzo, A.L., Barberi, F., Carapezza, M.I., De Astis, G., Romano, C., Sortino, F., 2015. Geochemistry of the mantle source and magma feeding system beneath Turrialba volcano, Costa Rica. Lithos 232, 319–335.

Díaz, D., Heise, W., Zamudio, F., 2015. Three-dimensional resistivity image of the magmatic system beneath Lastarria volcano and evidence for magmatic intrusion in the back arc (northern Chile). Geophys. Res. Lett. 42 (13), 5212–5218.

Faccini, B., Rizzo, A.L., Bonadiman, C., Ntaflos, T., Seghedi, I., Grégoire, M., Ferretti, G., Coltorti, M., 2020. Subduction-related melt refertilisation and alkaline metasomatism in the Eastern Transylvanian Basin lithospheric mantle: Evidence from mineral chemistry and noble gases in fluid inclusions. Lithos 105516.

Feeley, T.C., 1993. Volcán Ollagüe: Volcanology, petrology, and geochemistry of a major Quaternary volcanic center in the central Andes. Ph. D. thesis. University of California, Los Angeles.

Feeley, T.C., Davidson, J.P., 1994. Petrology of calc-alkaline lavas at volc´ n ollagüe and the origin of compositional diversity at central Andean Stratovolcanoes. J. Petrol. 35 (5), 1295–1340.

Figueroa, J., 2006. Petrografia, mineralogia y geoquiica de las lavas del volcan Sairecabur (22°44′ - 67°53′), region de Antofagasta. Universidad de Concepcion, Chile.

Froger, J.L., Rémy, D., Bonvalot, S., Legrand, D., 2007. Two scales of inflation at Lastarria-Cordon del Azufre volcanic complex, central Andes, revealed from ASAR-ENVISAT interferometric data. Earth Planet. Sci. Lett. 255 (1–2), 148–163.

Gaete Rojas, A.B., Walter, T.R., Bredemeyer, S., Zimmer, M., Kujawa, C., Franco Marin, L., San Martin, J., Bucarey Parra, C., 2020. Processes culminating in the 2015 phreatic explosion at Lascar volcano, Chile, evidenced by multiparametric data. Nat. Hazards Earth Syst. Sci. (NHESS) 20 (2), 377–397.

Gaete, A., Cesca, S., Franco, L., San Martin, J., Cartes, C., Walter, T.R., 2019. Seismic activity during the 2013–2015 intereruptive phase at Lascar volcano, Chile. Geophys. J. Int. 219 (1), 449–463.

Gardeweg, M.C., Medina, E., 1994, October. La erupción subpliniana del 19–20 de Abril de 1993 del volcan Lascar, N de Chile. Actas 7° Congreso Geologico Chileno. Vol. 1, pp. 299–304.

Gardeweg, M.C., Sparks, R.S.J., Matthews, S.J., 1998. Evolution of Lascar volcano, northern Chile. J. Geol. Soc. London 155 (1), 89–104.

Gardeweg, M., Chile, Servicio Nacional de Geología y Minería, & Gardeweg, 2011. Geología del Volcán Láscar: región de Antofagasta. Servicio Nacional de Geología y Minería.

Global Volcanism Program, 1993. Report on Lascar (Chile). In: Venzke, E. (Ed.), Bulletin of the Global Volcanism Network, 18:4. Smithsonian Institution. https://doi.org/10.5479/si.GVP.BGVN199304-355100.

Global Volcanism Program, 1994. Report on Lascar (Chile). In: Wunderman, R. (Ed.), Bulletin of the Global Volcanism Network, 19:7. Smithsonian Institution. https://doi.org/10.5479/si.GVP.BGVN199407-355100.

Global Volcanism Program, 1996. Report on Lascar (Chile). In: Wunderman, R. (Ed.), Bulletin of the Global Volcanism Network, 21:7. Smithsonian Institution. https://doi.org/10.5479/si.GVP.BGVN199607-355100.

Global Volcanism Program, 2015. Report on Lascar (Chile). In: Venzke, E. (Ed.), Bulletin of the Global Volcanism Network, 40:6. Smithsonian Institution. https://doi.org/10.5479/si.GVP.BGVN201506-355100.

Global Volcanism Program, 2017. Report on Lascar (Chile). In: Crafford, A.E., Venzke, E. (Eds.), Bulletin of the Global Volcanism Network, 42:7. Smithsonian Institution. https://doi.org/10.5479/si.GVP.BGVN201707-355100.
Global Volcanism Program, 2018. Report on Lascar (Chile). In: Sennert, S.K. (Ed.), Weekly Volcanic Activity Report, 4 April-10 April 2018. Smithsonian Institution and US Geological Survey.
Godoy, B., 2014. Evolución petrológica de la Cadena Volcánica San Pedro-Linzor (21 30′ S–22 10′ S), norte de Chile, y su relación con la geodinámica Andina. Doctoral dissertation Dissertation, Ph. D. Thesis. Universidad Católica del Norte, Chile.
Godoy, B., Wörner, G., Kojima, S., Aguilera, F., Simon, K., Hartmann, G., 2014. Low-pressure evolution of arc magmas in thickened crust: The San Pedro–Linzor volcanic chain, Central Andes, northern Chile. J. South Am. Earth Sci. 52, 24–42.
Godoy, B., Taussi, M., González-Maurel, O., Renzulli, A., Hernández-Prat, L., le Roux, P., Morata, D., Menzies, A., 2019. Linking the mafic volcanism with the magmatic stages during the last 1 Ma in the main volcanic arc of the Altiplano-Puna Volcanic Complex (Central Andes). J. South Am. Earth Sci. 102295.
González-Ferrán, O., 1995. Volcanes de Chile. Instituto geográfico militar, Santiago, p. 635.
Graham, D.W., 2002. Noble gas isotope geochemistry of mid-ocean ridge and ocean island basalts: Characterization of mantle source reservoirs. Rev. Mineral. Geochem. 47 (1), 247–317.
Grunder, A.L., Klemetti, E.W., Feeley, T.C., McKee, C.M., 2008. Eleven million years of arc volcanism at the Aucanquilcha Volcanic Cluster, northern Chilean Andes: Implications for the life span and emplacement of plutons. Earth Environ. Sci. Trans. R. Soc. Edinb. 97 (4), 415–436.
Harmon, R.S., Barreiro, B.A., Moorbath, S., Hoefs, J., Francis, P.W., Thorpe, R.S., Deruelle, B., McHugh, J., Viglino, J.A., 1984. Regional O-, Sr-, and Pb-isotope relationships in late Cenozoic calc-alkaline lavas of the Andean Cordillera. J. Geol. Soc. London 141 (5), 803–822.
Haschke, M., Günther, A., Melnick, D., Echtler, H., Reutter, K.J., Scheuber, E., Oncken, O., 2006. Central and southern Andean tectonic evolution inferred from arc magmatism. The Andes. Springer, Berlin, Heidelberg, pp. 337–353.
Hickey, R.L., Frey, F.A., Gerlach, D.C., Lopez-Escobar, L., 1986. Multiple sources for basaltic arc rocks from the southern volcanic zone of the Andes (34–41 S): Trace element and isotopic evidence for contributions from subducted oceanic crust, mantle, and continental crust. J. Geophys. Res. Solid Earth 91 (B6), 5963–5983.
Hildreth, W., Moorbath, S., 1988. Crustal contributions to arc magmatism in the Andes of central Chile. Contrib. Mineral. Petrol. 98 (4), 455–489.
Hilton, D.R., Hammerschmidt, K., Teufel, S., Friedrichsen, H., 1993. Helium isotope characteristics of Andean geothermal fluids and lavas. Earth Planet. Sci. Lett. 120 (3–4), 265–282.
Hilton, D.R., Fischer, T.P., Marty, B., 2002. Noble gases and volatile recycling at subduction zones. Rev. Mineral. Geochem. 47 (1), 319–370.
Hoffmann, C., 2011. Petrografia y geoqumica de los conos del campo de lavas negro de aras (23°57′ -24°26' Lat. S. y 67°57′ - 68°42′ Long. O.) al norte del volcan Socompa, II region de Antofagasta, Chile.
Hoke, L., Hilton, D.R., Lamb, S.H., Hammerschmidt, K., Friedrichsen, H., 1994. 3He evidence for a wide zone of active mantle melting beneath the Central Andes. Earth Planet. Sci. Lett. 128 (3–4), 341–355.
Hopp, J., Ionov, D.A., 2011. Tracing partial melting and subduction-related metasomatism in the Kamchatkan mantle wedge using noble gas compositions. Earth Planet. Sci. Lett. 302 (1–2), 121–131.
Hora, J.M., Singer, B.S., Wörner, G., 2007. Volcano evolution and eruptive flux on the thick crust of the Andean Central Volcanic Zone: 40Ar/39Ar constraints from Volcán Parinacota, Chile. GSA Bull. 119 (3–4), 343–362.
Howie, R.A., Zussman, J., Deer, W., 1992. An Introduction to the Rock-Forming Minerals. Longman, p. 696.
Iacono-Marziano, G., Paonita, A., Rizzo, A., Scaillet, B., Gaillard, F., 2010. Noble gas solubilities in silicate melts: New experimental results and a comprehensive model of the effects of liquid composition, temperature and pressure. Chem. Geol. 279 (3–4), 145–157.
Jacques, G., Hoernle, K., Gill, J., Wehrmann, H., Bindeman, I., Lara, L.E., 2014. Geochemical variations in the Central Southern Volcanic Zone, Chile (38–43 S): The role of fluids in generating arc magmas. Chem. Geol. 371, 27–45.
Kay, S.M., Mpodozis, C., Gardeweg, M., 2014. Magma sources and tectonic setting of Central Andean andesites (25.5–28 S) related to crustal thickening, forearc subduction erosion and delamination. Geol. Soc. Lond. Spec. Publ. 385 (1), 303–334.
Kiebala, A., 2008. Magmatic processes by U-Th disequilibria method. Comparison of Two Andean Systems: El Misti (S. Peru) and Taapaca Volcanic Center (N. Chile). Ph. D. thesis. Georg August Universität, Göttingen.
Kobayashi, M., Sumino, H., Nagao, K., Ishimaru, S., Arai, S., Yoshikawa, M., Kawamoto, T., Kumagai, Y., Kobayashi, T., Burgess, R., Ballentine, C.J., 2017. Slab-derived halogens and noble gases illuminate closed system processes controlling volatile element transport into the mantle wedge. Earth Planet. Sci. Lett. 457, 106–116.
Kohlbach, I., Lohnert, E., 1999. Geological Map of Taapaca Volcano and Adjacent Areas (North Chile) 1:25 000. Diploma Mapping Thesis. Georg-August Universität Göttingen.
Kurz, M.D., 1986. Cosmogenic helium in a terrestrial igneous rock. Nature 320 (6061), 435–439.
Lamb, S., Hoke, L., 2007. Cenozoic behind Arc Volcanism in the Bolivian Andes, South America: Implications for mantle melt generation and litosphere structure. J. Geol. Soc. 2007 (v164), 795–814.
Lange, R.A>, Frey, H.M., Hector, J., 2009. A thermodynamic model for the plagioclase-liquid hygrometer/thermometer. Am. Mineral. 94 (4), 494–506.
Layana, S., Aguilera, F., Rojo, G., Vergara, A., Salazar, P., Quispe, J., Urrra, P., Urrutia, D., 2020. Volcanic Anomalies monitoring System (VOLCANOMS), a low-cost volcanic monitoring system based on Landsat images. Remote Sensing 12 (10), p.1589.
Linsley, D.H., 1983. Pyroxene thermometer. Am. Mineral. 68, 477–493.
Lopez, T., Aguilera, F., Tassi, F., de Moor, J.M., Bobrowski, N., Aiuppa, A., Tamburello, G., Rizzo, A.L., Liuzzo, M., Viveiros, F., Cardellini, C., 2018. New insights into the magmatic-hydrothermal system and volatile budget of Lastarria volcano, Chile: Integrated results from the 2014 IAVCEI CCVG 12th Volcanic Gas Workshop. Geosphere 14 (3), 983–1007.
Mamani, M., Tassara, A., Wörner, G., 2008. Composition and structural control of crustal domains in the central Andes. Geochem. Geophys. Geosyst. 9 (3).
Mamani, M., Wörner, G., Sempere, T., 2010. Geochemical variations in igneous rocks of the Central Andean orocline (13 S to 18 S): Tracing crustal thickening and magma generation through time and space. Geol. Soc. Am. Bull. 122 (1–2), 162–182.
Marsh, B.D., 1998. On the interpretation of crystal size distributions in magmatic systems. J. Petrol. 39 (4), 553–599.
Marsh, B.D., 2013. On some fundamentals of igneous petrology. Contrib. Mineral. Petrol. 166 (3), 665–690.
Martelli, M., Rizzo, A.L., Renzulli, A., Ridolfi, F., Arienzo, I., Rosciglione, A., 2014. Noble-gas signature of magmas from a heterogeneous mantle wedge: The case of Stromboli volcano (Aeolian Islands, Italy). Chem. Geol. 368, 39–53.
Marty, B., 2012. The origins and concentrations of water, carbon, nitrogen and noble gases on Earth. Earth Planet. Sci. Lett. 313, 56–66.
Matthews, S.J., Jones, A.P., Gardeweg, M.C., 1994. Lascar Volcano, Northern Chile; evidence for steady-state disequilibrium. J. Petrol. 35 (2), 401–432.
Matthews, S.J., Gardeweg, M.C., Sparks, R.S.J., 1997. The 1984 to 1996 cyclic activity of Lascar Volcano, northern Chile: Cycles of dome growth, dome subsidence, degassing and explosive eruptions. Bull. Volcanol. 59 (1), 72–82.
Matthews, S.J., Sparks, R.S.J., Gardeweg, M.C., 1999. The Piedras Grandes–Soncor eruptions, Lascar volcano, Chile; evolution of a zoned magma chamber in the central Andean upper crust. J. Petrol. 40 (12), 1891–1919.
Mattioli, M., Renzulli, A., Menna, M., Holm, P.M., 2006. Rapid ascent and contamination of magmas through the thick crust of the CVZ (Andes, Ollagüe region): Evidence from a nearly aphyric high-K andesite with skeletal olivines. J. Volcanol. Geotherm. Res. 158 (1–2), 87–105.
Menard, G., Moune, S., Vlastélic, I., Aguilera, F., Valade, S., Bontemps, M., González, R., 2014. Gas and aerosol emissions from Lascar volcano (Northern Chile): Insights into the origin of gases and their links with the volcanic activity. J. Volcanol. Geotherm. Res. 287, 51–67.
Naranjo, J.A., 1992. Chemistry and petrological evolution of the Lastarria volcanic complex in the north Chilean Andes. Geol. Mag. 129 (06), 723–740.
Naranjo, J.A., 2010. Geología del Complejo Volcánico Lastarria, Región de Antofagasta. Servicio Nacional de Geología y Minería, Carta Geológica de Chile, Serie Geología Básica 123: 33p., 1 mapa escala 1:25.000. Santiago.
Nuccio, P.M., Paonita, A., Rizzo, A., Rosciglione, A., 2008. Elemental and isotope covariation of noble gases in mineral phases from Etnean volcanics erupted during 2001–2005, and genetic relation with peripheral gas discharges. Earth Planet. Sci. Lett. 272 (3–4), 683–690.
Oppenheimer, C., Fischer, T.P., Scaillet, B., 2014. Volcanic Degassing: Process and Impact.
Ortega, V., 2008. Estudio petrografico y petrologico de las rocas volcanicas de los volcanes Lascar. Tilocalar Norte y Tilocalar Sur.
Ozima, M., Podosek, F.A., 2002. Noble Gas Geochemistry. Cambridge University Press.
Patino, L.C., Carr, M.J., Feigenson, M.D., 2000. Local and regional variations in Central American arc lavas controlled by variations in subducted sediment input. Contrib. Mineral. Petrol. 138 (3), 265–283.
Plank, T., 2014. The chemical composition of subducting sediments. In: Keeling, R.F. (Ed.), Treatise on Geochemistry, 2. ed Elsevier, Amsterdam, pp. 607–629. https://doi.org/10.1016/B978-0-08-095975-7.00319-3.
Plank, T., Langmuir, C.H., 1998. The chemical composition of subducting sediment and its consequences for the crust and mantle. Chem. Geol. 145 (3–4), 325–394.
Pritchard, M.E., Simons, M., 2002. A satellite geodetic survey of large-scale deformation of volcanic centres in the central Andes. Nature 418 (6894), 167.
Pritchard, M.E., Simons, M., 2004. An InSAR-based survey of volcanic deformation in the central Andes. Geochem. Geophys. Geosyst. 5 (2).
Protin, M., Blard, P.H., Marrocchi, Y., Mathon, F., 2016. Irreversible adsorption of atmospheric helium on olivine: A lobster pot analogy. Geochim. Cosmochim. Acta 179, 76–88.
Putirka, K.D., 2005. Igneous thermometers and barometers based on plagioclase+ liquid equilibria: Tests of some existing models and new calibrations. Am. Mineral. 90 (2–3), 336–346.
Putirka, K.D., 2008. Thermometers and barometers for volcanic systems. Rev. Mineral. Geochem. 69 (1), 61–120.
Putirka, K.D., Mikaelian, H., Ryerson, F., Shaw, H., 2003. New clinopyroxene-liquid thermobarometers for mafic, evolved, and volatile-bearing lava compositions, with applications to lavas from Tibet and the Snake River Plain, Idaho. Am. Mineral. 88 (10), 1542–1554.
Ray, M.C., Hilton, D.R., Muñoz, J., Fischer, T.P., Shaw, A.M., 2009. The effects of volatile recycling, degassing and crustal contamination on the helium and carbon geochemistry of hydrothermal fluids from the Southern Volcanic Zone of Chile. Chem. Geol. 266 (1), 38–49.
Remy, D., Froger, J.L., Perfettini, H., Bonvalot, S., Gabalda, G., Albino, F., Cayol, V., Legrand, D., Saint Blanquat, M.D., 2014. Persistent uplift of the l azufre volcanic complex (c entral a ndes): New insights from PCAIM inversion of inSAR time series and GPS data. Geochem. Geophys. Geosyst. 15 (9), 3591–3611.

Ridolfi, F., Renzulli, A., 2012. Calcic amphiboles in calc-alkaline and alkaline magmas: Thermobarometric and chemometric empirical equations valid up to 1,130° C and 2.2 GPa. Contrib. Mineral. Petrol. 163 (5), 877–895.
Ridolfi, F., Renzulli, A., Puerini, M., 2010. Stability and chemical equilibrium of amphibole in calc-alkaline magmas: An overview, new thermobarometric formulations and application to subduction-related volcanoes. Contrib. Mineral. Petrol. 160 (1), 45–66.
Rizzo, A., Barberi, F., Carapezza, M.L., Di Piazza, A., Francalanci, L., Sortino, F., D'Alessandro, W., 2015. New mafic magma refilling a quiescent volcano: Evidence from He–Ne–Ar isotopes during the 2011–2012 unrest at Santorini, Greece. Geochem. Geophys. Geosyst. 16 (3), 798–814.
Rizzo, A.L., Caracausi, A., Chavagnac, V., Nomikou, P., Polymenakou, P.N., Mandalakis, M., Kotoulas, G., Magoulas, A., Castillo, A., Lampridou, D., 2016. Kolumbo submarine volcano (Greece): An active window into the Aegean subduction system. Sci. Rep. 6 (1), 1–9.
Rizzo, A.L., Pelorosso, B., Coltorti, M., Ntaflos, T., Bonadiman, C., Matusiak-Małek, M., Italiano, F., Bergonzoni, G., 2018. Geochemistry of noble gases and CO2 in fluid inclusions from lithospheric mantle beneath Wilcza Góra (Lower Silesia, southwest Poland). Front. Earth Sci. 6, 215.
Rizzo, A.L., Caracausi, A., Chavagnac, V., Nomikou, P., Polymenakou, P., Mandalakis, M., Kotoulas, G., Magoulas, A., Castillo, A., Lampridou, D., Marusczak, N., 2019. Geochemistry of CO2-rich gases venting from submarine volcanism: The case of Kolumbo (Hellenic Volcanic Arc, Greece). Front. Earth Sci 7, 60.
Robidoux, P., Aiuppa, A., Rotolo, S., Hauri, E.H., Rizzo, A.-L., Frezzotti, M.L., 2017. The volatile content of mafic-to-intermediate magmas from San Cristóbal volcano, Nicaragua. Lithos 272-273, 147–163.
Roedder, E., 1979. Origin and significance of magmatic inclusions. Bull. Mineral. 102 (5), 487–510.
Roedder, E., 1984. Volume 12: Fluid inclusions. Rev. Miner. 12.
Rosner, M., Erzinger, J., Franz, G., Trumbull, R.B., 2003. Slab-derived boron isotope signatures in arc volcanic rocks from the Central Andes and evidence for boron isotope fractionation during progressive slab dehydration. Geochem. Geophys. Geosyst. 4 (8).
Roulleau, E., Tardani, D., Sano, Y., Takahata, N., Vinet, N., Bravo, F., Muñoz, C., Sanchez, J., 2016. New insight from noble gas and stable isotopes of geothermal/hydrothermal fluids at Caviahue-Copahue Volcanic Complex: Boiling steam separation and water-rock interaction at shallow depth. J. Volcanol. Geotherm. Res. 328, 70–83.
Roulleau, E., Tardani, D., Vlastelic, I., Vinet, N., Sanchez, J., Sano, Y., Takahata, N., 2018. Multi-element isotopic evolution of magmatic rocks from Caviahue-Copahue Volcanic Complex (Chile-Argentina): Involvement of mature slab recycled materials. Chem. Geol. 476, 370–388.
Ruch, J., Manconi, A., Zeni, G., Solaro, G., Pepe, A., Shirzaei, M., Walter, T.R., Lanari, R., 2009. Stress transfer in the Lazufre volcanic area, central Andes. Geophys. Res. Lett. 36 (22).
Sadofsky, S.J., Portnyagin, M., Hoernle, K., van den Bogaard, P., 2008. Subduction cycling of volatiles and trace elements through the central American volcanic arc: Evidence from melt inclusions. Contrib. Mineral. Petrol. 155 (4), 433–456.
Salters, V.J., Stracke, A., 2004. Composition of the depleted mantle. Geochem. Geophys. Geosyst. 5 (5).
Sano, Y., Fischer, T.P., 2013. The analysis and interpretation of noble gases in modern hydrothermal systems. The noble gases as geochemical tracers. Springer, Berlin, Heidelberg, pp. 249–317.
Sano, Y., Wakita, H., 1985. Geographical distribution of 3He/4He ratios in Japan: Implications for arc tectonics and incipient magmatism. J. Geophys. Res. Solid Earth 90 (B10), 8729–8741.
Sano, Y., Gamo, T., Williams, S.N., 1997. Secular variations of helium and carbon isotopes at Galeras volcano, Colombia. J. Volcanol. Geotherm. Res. 77 (1–4), 255–265.
Scheinost, A., 2018. Variaciones geoquímicas e isotópicas de la Zona Volcánica Central (ZVC) del norte de Chile entre los 17.5 y 27.2 S. Undergraduate Thesis. Universidad Católica del Norte, Chile.
Scott, E.M., Allen, M.B., Macpherson, C.G., McCaffrey, K.J., Davidson, J.P., Saville, C., Ducea, M.N., 2018. Andean surface uplift constrained by radiogenic isotopes of arc lavas. Nat. Commun. 9 (1), 1–8.
Sepúlveda, F., Lahsen, A., Powell, T., 2007. Gas geochemistry of the Cordón Caulle geothermal system, Southern Chile. Geothermics 36 (5), 389–420.
Shaw, A.M., Hilton, D.R., Fisher, T.P., Walker, J.A., Alvarado, G.E., 2003. Contrasting He–C relationships in Nicaragua and Costa Rica: Insights into C cycling through subduction zones. Earth Planet. Sci. Lett. 214, 419–513.
Shaw, A.M., Hilton, D.R., Fisher, T.P., Walker, J.A., de Leew, G.A.M., 2006. Helium isotope variations in mineral separates from Costa Rica and Nicaragua: Assessing crustal contributions, timescale variations and diffusion-related mechanism. Chem. Geol. 230, 124–139.
Sparks, R.S.J., Gardeweg, M.C., Calder, E.S., Matthews, S.J., 1997. Erosion by pyroclastic flows on Lascar Volcano, Chile. Bull. Volcanol. 58 (7), 557–565.
Spica, Z., Legrand, D., Iglesias, A., Walter, T.R., Heimann, S., Dahm, T., Froger, J.L., Rémy, D., Bonvalot, S., West, M., Pardo, M., 2015. Hydrothermal and magmatic reservoirs at Lazufre volcanic area, revealed by a high-resolution seismic noise tomography. Earth Planet. Sci. Lett. 421, 27–38.
Stechern, A., Just, T., Holtz, F., Blume-Oeste, M., Namur, O., 2017. Decoding magma plumbing and geochemical evolution beneath the Lastarria volcanic complex (Northern Chile)—Evidence for multiple magma storage regions. J. Volcanol. Geotherm. Res. 338, 25–45.
Stern, C.R., 2004. Active Andean volcanism: its geologic and tectonic setting. Rev. Geol. Chile 31 (2), 161–206.
Tamburello, G., Hansteen, T.H., Bredemeyer, S., Aiuppa, A., Tassi, F., 2014. Gas emissions from five volcanoes in northern Chile and implications for the volatiles budget of the Central Volcanic Zone. Geophys. Res. Lett. 41 (14), 4961–4969.
Taran, Y.A., 2009. Geochemistry of volcanic and hydrothermal fluids and volatile budget of the Kamchatka–Kuril subduction zone. Geochim. Cosmochim. Acta 73 (4), 1067–1094.
Tardani, D., Reich, M., Roulleau, E., Takahata, N., Sano, Y., Pérez-Flores, P., Sánchez-Alfaro, P., Cembrano, J., Arancibia, G., 2016. Exploring the structural controls on helium, nitrogen and carbon isotope signatures in hydrothermal fluids along an intra-arc fault system. Geochim. Cosmochim. Acta 184, 193–211.
Tassi, F., Aguilera, F., Vaselli, O., Medina, E., Tedesco, D., Huertas, A.D., Poreda, R., Kojima, S., 2009. The magmatic-and hydrothermal-dominated fumarolic system at the Active Crater of Lascar volcano, northern Chile. Bull. Volcanol. 71 (2), 171–183.
Tassi, F., Aguilera, F., Vaselli, O., Darrah, T., Medina, E., 2011. Gas discharges from four remote volcanoes in northern Chile (Putana, Olca, Irruputuncu and Alitar): A geochemical survey. Ann. Geophys. 54 (2).
Tassi, F., Aguilera, F., Benavente, O., Paonita, A., Chiodini, G., Caliro, S., Agusto, M., Gutierrez, F., Capaccioni, B., Vaselli, O., Caselli, A., 2016. Geochemistry of fluid discharges from Peteroa volcano (Argentina-Chile) in 2010–2015: Insights into compositional changes related to the fluid source region (s). Chem. Geol. 432, 41–53.
Tassi, F., Agusto, M., Lamberti, C., Caselli, A.T., Pecoraino, G., Caponi, C., Szentiványi, J., Venturi, S., Vaselli, O., 2017. The 2012–2016 eruptive cycle at Copahue volcano (Argentina) versus the peripheral gas manifestations: Hints from the chemical and isotopic features of fumarolic fluids. Bull. Volcanol. 79 (10), 69.
Thorpe, R.S., 1982. The Andes. Andesites: Orogenic andesites and related rocks, pp. 187–205.
Thorpe, R.S., 1984. The tectonic setting of active Andean volcanism. Andean magmatism. Birkhäuser, Boston, pp. 4–8.
Thorpe, R.S., Francis, P.W., 1979. Petrogenetic relationships of volcanic and intrusive rocks of the Andes. In: (Eds.), Origin of Granite Batholiths. Birkhäuser, Boston, p. 65.
Trumbull, R.B., Wittenbrink, R., Hahne, K., Emmermann, R., Büsch, W., Gerstenberger, H., Siebel, W., 1999. Evidence for Late Miocene to recent contamination of arc andesites by crustal melts in the Chilean Andes (25–26 S) and its geodynamic implications. J. South Am. Earth Sci. 12 (2), 135–155.
Turner, S., Hawkesworth, C., 1998. Using geochemistry to map mantle flow beneath the Lau Basin. Geology 26 (11), 1019–1022.
Ureta, G., 2015. Evolucion geologica y petrologica del volcan Cerro Overo (23°31'S-67°39'W), Region de Antofagasta, Chile. Universidad Catolica del Norte, departamento de ciencias Geologicas.
Veloso, E.E., Tardani, D., Elizalde, D., Godoy, B.E., Sánchez-Alfaro, P.A., Aron, F., Reich, M., Morata, D., 2019. A review of the geodynamic constraints on the development and evolution of geothermal systems in the Central Andean Volcanic Zone (18–28° Lat. S). Internat. Geol. Rev. 1–25.
Völker, D., Geersen, J., Contreras-Reyes, E., Reichert, C., 2013. Sedimentary fill of the Chile Trench (32–46° S): Volumetric distribution and causal factors. J. Geol. Soc. London 170 (5), 723–736.
Wittenbrink, R., 1997. Zeitliche Variationen der Magmengenese miozäner bis quartärer Vulkanite im südlichen Bereich der Zentralen vulkanischen Zone der Anden (CVZ, 25°–26°S, 67°–69°W) (in German with English summary), Berliner Geowissenschaftliche Abhandlungen, Reihe A 193. Freie Univ, p. 135.
Workman, R.K., Hart, S.R., 2005. Major and trace element composition of the depleted MORB mantle (DMM). Earth Planet. Sci. Lett. 231 (1–2), 53–72.
Wörner, G., Harmon, R.S., Davidson, J., Moorbath, S., Turner, D.L., McMillan, N., Nyes, C., Lopez-Escobar, L., Moreno, H., 1988. The nevados de payachata volcanic region (18 S/69 W, N. Chile). Bull. Volcanol. 50 (5), 287–303.
Wörner, G., Moorbath, S., Horn, S., Entenmann, J., Harmon, R.S., Davidson, J.P., Lopez-Escobar, L., 1994. Large-and fine-scale geochemical variations along the Andean arc of northern Chile (17.5–22 S). Tectonics of the southern Central Andes. Springer, Berlin, Heidelberg, pp. 77–92.
Wörner, G., Mamani, M., Blum-Oeste, M., 2018. Magmatism in the central Andes. Elements Int. Mag. Mineral. Geochem. Petrol. 14 (4), 237–244.
Yamamoto, J., Kaneoka, I., Nakai, S.I., Kagi, H., Prikhod'ko, V.S., Arai, S., 2004. Evidence for subduction-related components in the subcontinental mantle from low 3He/4He and 40Ar/36Ar ratio in mantle xenoliths from Far Eastern Russia. Chem. Geol. 207 (3–4), 237–259.